JBC RESEARCH ARTICLE

Identification of novel plant cysteine oxidase inhibitors from a yeast chemical genetic screen

Received for publication, July 14, 2023, and in revised form, September 28, 2023 Published, Papers in Press, October 19, 2023,
https://doi.org/10.1016/j.jbc.2023.105366

Mikel Lavilla-Puerta[1], Rebecca Latter[2], Francesca Bellè[3], Tiziana Cervelli[3], Alvaro Galli[3], Pierdomenico Perata[1], Andrea Chini[4], Emily Flashman[5], and Beatrice Giuntoli[1,6,*]

From the [1]Plantlab, Center of Plant Sciences, Scuola Superiore Sant'Anna, Pisa, Italy; [2]Department of Chemistry, University of Oxford, Oxford, UK; [3]Clinical Physiology Institute, CNR, Pisa, Italy; [4]Department of Plant Molecular Genetics, Centro Nacional de Biotecnología, CSIC, Madrid, Spain; [5]Department of Biology, University of Oxford, Oxford, UK; [6]Biology Department, University of Pisa, Pisa, Italy

Reviewed by members of the JBC Editorial Board. Edited by Sarah E. O'Connor

Hypoxic responses in plants involve Plant Cysteine Oxidases (PCOs). They catalyze the N-terminal cysteine oxidation of Ethylene Response Factors VII (ERF-VII) in an oxygen-dependent manner, leading to their degradation *via* the cysteine N-degron pathway (Cys-NDP) in normoxia. In hypoxia, PCO activity drops, leading to the stabilization of ERF-VIIs and subsequent hypoxic gene upregulation. Thus far, no chemicals have been described to specifically inhibit PCO enzymes. In this work, we devised an *in vivo* pipeline to discover Cys-NDP effector molecules. Budding yeast expressing AtPCO4 and plant-based ERF-VII reporters was deployed to screen a library of natural-like chemical scaffolds and was further combined with an Arabidopsis Cys-NDP reporter line. This strategy allowed us to identify three PCO inhibitors, two of which were shown to affect PCO activity *in vitro*. Application of these molecules to Arabidopsis seedlings led to an increase in ERF-VII stability, induction of anaerobic gene expression, and improvement of tolerance to anoxia. By combining a high-throughput heterologous platform and the plant model Arabidopsis, our synthetic pipeline provides a versatile system to study how the Cys-NDP is modulated. Its first application here led to the discovery of at least two hypoxia-mimicking molecules with the potential to impact plant tolerance to low oxygen stress.

Oxygen is essential to most eukaryotes as the terminal acceptor of mitochondrial electron transport, beyond serving as a substrate for numerous reactions. Aerobic organisms have therefore evolved specific mechanisms to sense and adapt to decreases from the normal partial pressure of oxygen to attune energy homeostasis with physiology. Restrictions to oxygen availability may occur in specific environments or within tissues, where hypoxia is linked to pathological conditions or, in other cases, to the maintenance of specific developmental niches (1–3).

Direct oxygen perception takes place in both animals and plants, where prolyl hydroxylases (PHDs) and plant cysteine oxidases (PCOs), respectively, have been identified as oxygen-sensing enzymes (4, 5). These non-heme iron-dependent dioxygenases, although phylogenetically unrelated, fulfill analogous roles in their respective pathways, by connecting the addition of molecular oxygen to target proteins to their ubiquitination and processing through the 26S proteasome (6–9). In animals, PHDs catalyze hydroxylation of one or both conserved prolyl residues in the α-subunits of the Hypoxia Inducible Factors (HIF1α and HIF2α) to trigger ubiquitination while, in plants, PCOs catalyze oxidation of N-terminally exposed Cys residues in proteins, generated after methionine removal or endoproteolytic protein cleavage. Nt-Cys oxidized proteins are channeled to the arginine N-degron pathway, a dedicated degradation pathway that comprises the sequential action of Arginyl t-RNA Transferases (ATE) and PRT6-type E3 ligases and the proteasome (10); the main substrates of this pathway in plants are the ERF-VII subfamily of ethylene-responsive transcription factors. Hypoxia leads to a drop in PHD or PCO activity, preventing the degradation of HIFα or ERF-VIIs and thereby enabling their accumulation in the nucleus, where they act as master regulators of low-oxygen responsive genes in their respective organisms (11–13). In multicellular eukaryotes, therefore, oxygen sensing deploys a conserved regulatory scheme based on the O_2-dependent conditional degradation of key signaling factors directly connecting physiological responses to oxygen fluctuations (14, 15).

The affinity for oxygen as a co-substrate of PHD and PCO enzymes lies within a range of concentrations compatible with tissue and subcellular oxygen levels; therefore, PHDs and PCOs can act as mediators of physiological responses to oxygen fluctuations (16, 17). Comprehensive kinetic characterization of *Arabidopsis thaliana* PCOs has indeed shown that their K_MO_2 span from 5 to 17% O_2 (5). It is therefore conceivable that PCO activities may vary over the full range of oxygen levels observed in plant tissues (from 21% in fully oxygenated tissues, down to below 1% O_2 in compact structures and fast-dividing districts) (2, 18, 19).

Several studies in humans have identified molecules that can reduce the Fe(II) and 2-oxoglutarate (2-OG)-dependent activity of the PHDs and, thereby, stabilize HIFα factors. So far,

* For correspondence: Beatrice Giuntoli, beatrice.giuntoli@unipi.it.

© 2023 THE AUTHORS. Published by Elsevier Inc on behalf of American Society for Biochemistry and Molecular Biology. This is an open access article under the CC BY-NC-ND license (http://creativecommons.org/licenses/by-nc-nd/4.0/).

three categories of PHD inhibitors have been reported: (i) those which non-specifically chelate or compete with PHD-bound iron, such as dipyridyl (DIP), deferoxamine (DFO), L-mimosine or antagonizing ions including Co^{2+}, Cu^{2+} and Ni^{+} (20), (ii) simple 2-oxoglutarate (2-OG) analogs, such as dimethyloxalylglycine (DMOG) and 3,4-dihydroxybenzoate which are non-specific for the PHDs (21, 22), and (iii) more complex inhibitors that bind to both the active site metal and other regions of the PHD enzymes, conferring increased selectivity and often preventing substrate binding, including FG-4592 and Molidustat (23–25). While chemicals belonging to the first two categories have been reported to alter general iron and 2-OG homeostasis (22), drugs from the last category hold the greatest potential due to their selectivity for PHDs among 2-OG dioxygenases and thus minimize the probability of pleiotropic effects. Indeed, the FG-4592-based drug Roxadustat was the first commercially released hypoxia-mimetic molecule for medical use and has been deployed so far for the treatment of renal anemia (26, 27).

No chemicals that are able to alter the plant oxygen signaling pathway have been described yet. In contrast, specific genetic regulation of thiol dioxygenase activity has been reported; mutations in crucial residues of the PCO4 enzyme from *A. thaliana* are associated with sub-active or completely inactive isoforms, and plants bearing these variants show an increased expression of anaerobic genes and other phenotypical traits linked to hypoxia (28). Beyond genetic and structural modifications, it is possible to alter thiol dioxygenase activity by modulating the availability of the Fe^{2+} cofactor essential for catalysis (29): iron chelation with DIP or DFO has been effectively used to inhibit the human thiol dioxygenase ADO in cell tissue cultures (30). In Arabidopsis, moreover, inhibition of the oxygen sensing pathway has been achieved by imposing transient zinc excess conditions, which was interpreted as a consequence of iron replacement by Zn^{+} in the PCO catalytic site (31). However, non-specific iron chelating agents or high levels of antagonizing ions may cause undesired physiological mis-regulation, by indiscriminately blocking the plethora of Fe-dependent pathways of a cell. On the contrary, no small molecules able to alter PCO activity directly and selectively have been found to date.

The possibility of manipulating plant oxygen sensitivity may pave the way to improve the response to low oxygen-associated stresses, such as flooding or soil waterlogging. Stabilization or simple over-expression of the ERF-VII proteins has been frequently found to be associated with higher tolerance to hypoxic stresses. For instance, a barley *prt6* mutant could improve yield, chlorophyll content, and biomass under waterlogging in comparison with wild-type plants (32) and over-expression of the rice ERF-VII factors *ERF66* and *ERF67* promoted submergence survival of the sensitive accession TNG67 (33). On the other hand, constitutive expression of an O_2-insensitive version of the ERF-VII factor RAP2.12 in Arabidopsis led to an opposite outcome, impairing submergence tolerance (13), suggesting that uncontrolled accumulation of cysteine N-degron pathway substrates may be linked to fitness penalties. Moreover, genetic disruption of the pathway can lead to severe developmental abnormalities, as in the case of a quadruple *pco* mutant in Arabidopsis (30, 34). Instead, it is reasonable to expect that PCO inhibitors would act in a tunable and reversible manner on the hypoxic responses, by transiently down-regulating the oxygen-sensing pathway. In addition, the use of small molecules can be easily transferred to many different plant species (35).

In this study, we established an *in vivo* pipeline of chemical screening, based on budding yeast (*Saccharomyces cerevisiae*), for the identification of small molecules able to modulate the activity of the plant oxygen sensing pathway. Budding yeast serves as the ideal test organism in our pipeline by virtue of its amenability to high-throughput chemical-genetics screens, favored by the ease of transformation and selection, fast growth, high reproducibility, and genetic stability of this organism (36, 37). *S. cerevisiae* lacks PCO homologous enzymes, however, plant oxygen sensing can in principle be reconstructed by coupling the native arginine N-degron pathway of yeast with heterologous thiol dioxygenases. Indeed, we have recently demonstrated that such a synthetic cysteine N-degron pathway is sufficient to turn stable Cys-starting proteins into substrates for conditional O_2-dependent degradation in *S. cerevisiae* (38). In the "PCOff" pipeline presented here, yeast was exploited as a tool to survey a large panel of compounds *in vivo*, identify potential PCO inhibitors, and further subject them to biochemical characterization *in vitro* and functional validation in plants.

Results

Generation of a chemosensitive strain of S. cerevisiae *for* in vivo *high-throughput chemical screening*

The first goal of this study was to establish a yeast platform suitable for the chemical screening of small molecules with an impact on the activity of the cysteine N-degron pathway (hereafter, Cys-NDP). First, we had to devise a strategy to overcome the recalcitrance to chemical treatments of budding yeast, which is characterized by high resistance to multiple cytotoxic compounds present in the extracellular environment. Multi-drug resistance is conferred by ATP-binding cassette (ABC) transporters that promote the active efflux of xenobiotics and physiological substrates through the plasma membrane. Among these pleiotropic drug resistance (Pdr) efflux pumps, Pdr5p is a prominent and widely characterized member (39–41); higher chemical susceptibility has been described in *pdr5Δ* mutants (42, 43). Moreover, ergosterol in the plasma membrane hinders the transit of lipophilic substances (43) as demonstrated by the higher permeability of *erg6Δ* mutants (44, 45). To enhance yeast uptake and retention capacity of externally supplied chemicals, we, therefore, combined the knock-out mutations in *PDR5* and the ergosterol biosynthetic gene *ERG6* into a *pdr5Δ,erg6Δ* strain. Similar mutants in different background strains had been previously characterized by an increased chemical hypersensitivity (43, 46).

We adopted a homologous recombination strategy, the *Delitto Perfetto* approach (47), to remove the *ERG6* locus from

ASBMB

a *pdr5Δ* background, obtaining the *pdr5Δ,erg6Δ* strain (Fig. 1*A*). Although viable, *pdr5Δ,erg6Δ* showed higher sensitivity to transformation, with a drop of efficiency from approximately $0.8{\cdot}10^6$ to $2{\cdot}10^3$ UFC μg^{-1} DNA after chemical transformation with the PEG/LiAc method (Fig. S1*A*). This is compatible with existing evidence on different *erg* and *pdr* knock-out strains, which show decreased thermotolerance and are less likely to survive treatments with agents that disrupt their membranes (43, 48, 49).

To evaluate the drug susceptibility of the double mutant, we took advantage of a previously developed luminescent substrate DLOR (Dual Luciferase Oxygen Reporter), based on the Arabidopsis Cys-NDP target RAP2.12 (38). Here, a cysteine N-degron represented by the $RAP2.12_{2\text{-}28}$ fragment, starting with

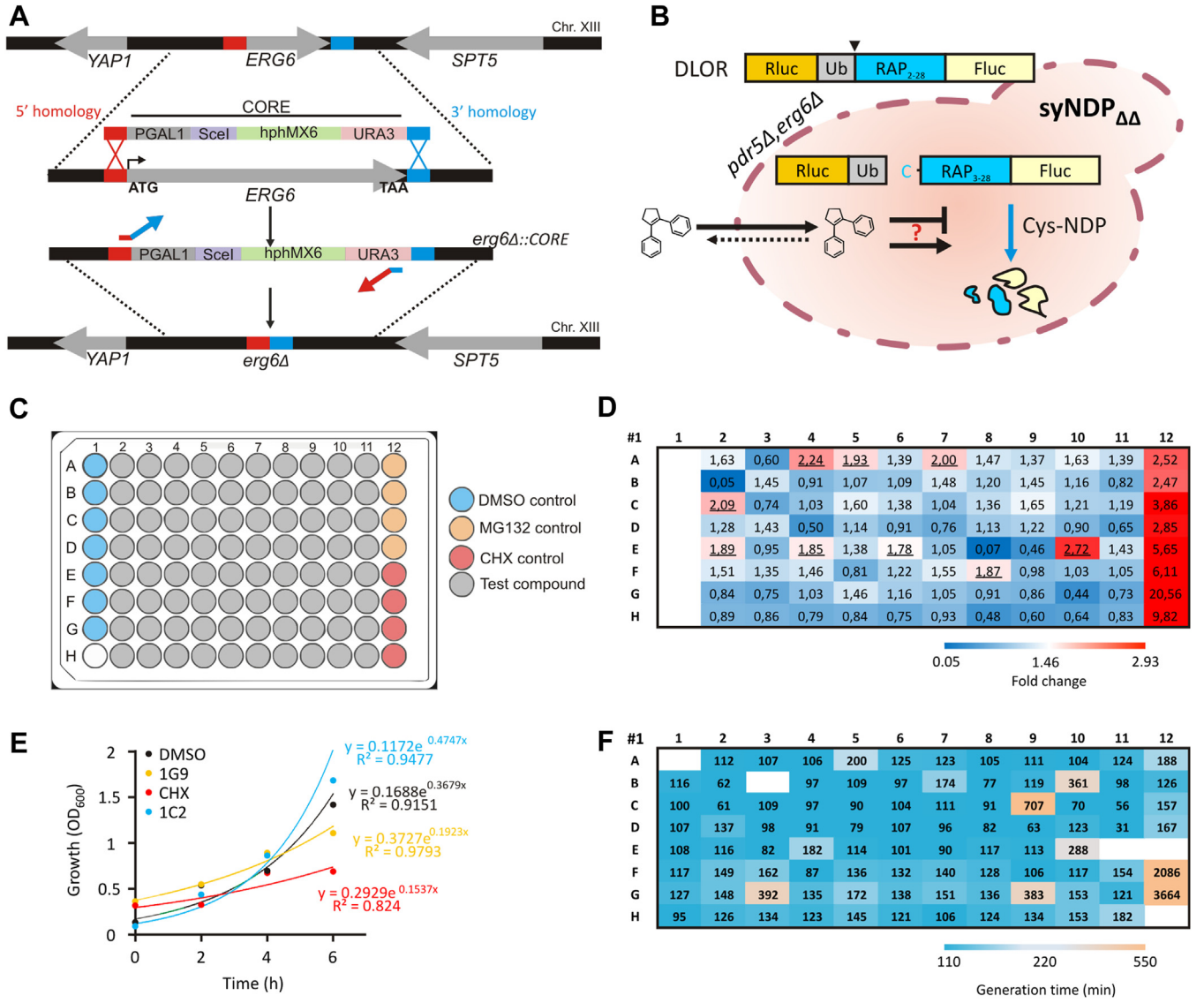

Figure 1. *In vivo* search for chemical effectors of the cysteine N-degron pathway with a yeast platform. *A*, deletion of the *S. cerevisiae ERG6* locus with the *Delitto Perfetto* strategy. *B*, schematic outline of the Cys-NDP reporter platform devised in this study. A synthetic cysteine N-degron pathway (Cys-NDP) was incorporated in the drug-sensitized *pdr5Δ,erg6Δ*, to obtain the "$synNDP_{\Delta\Delta}$" strain yeast strain, where proteasomal degradation of Cys-starting peptides is enabled thanks to the heterologous enzyme AtPCO4. This impinges on the native arginine N-degron pathway of yeast (38). The activity of the Cys-NDP pathway can be revealed by the stability of a genetically encoded reporter substrate, DLOR, and measured from its relative luciferase activity (Fluc/Rluc). DLOR harbors a ubiquitin cleavage site, indicated by the *black arrowhead*, that permits the post-translational generation of a cysteine N-degron. *C*, microtiter plate set-up adopted for the HTS platform. 200 µl of $synNDP_{\Delta\Delta}$ cell suspension at OD_{600} = 0.1 were dispensed in 96-well plate wells and supplemented with 1 µl DMSO (*blue*), MG132 (*orange*), cycloheximide (CHX, *red*), or different test compounds (*gray*). Clean media was dispensed in one well (*white*), to be used as a blank for spectrophotometric measurements. *D*, sample output plate from the screening (corresponding to plate 1). Fold change values indicate the variation in DLOR reporter activity (Fluc/Rluc ratio) from the average basal activity in DMSO-treated wells. Fold changes are represented as a three-colour scale where *blue* is the minimum fold change recorded on the plate, *red* is the average fold change from MG132-treated wells and *white* corresponds to 50% of the latter (values are specified below the color scale). *E*, growth (OD_{600}) profiles, over the total duration of the experiment (6 h), from three selected microcultures treated with CHX (*red*), compounds 1C2 (*cyan*) and 1G9 (*yellow*), or mock-treated cells from the same plate (*black line*). *F*, example of yeast generation times calculated during the chemical treatments between the 4 h and 6 h time points (data are from plate 1 of the screening). Data are represented as three-color scale where *blue* represents average generation times that are not different from the mock treatment, azure white shows generation times that are double that of the mock (taken as mild inhibition of growth) and *orange* represents generation times that are five times that of the mock (taken as slow cell division). Negative growth rates (associated with flattened growth curves such as CHX or 1G9 in Fig. 1*E*) were omitted (*white* wells).

its Cys2 residue, is incorporated in a ubiquitin fusion construct and becomes exposed by the action of endogenous deubiquitinating enzymes. The resulting reporter substrate can subsequently be degraded through the proteasome, upon expression of a cognate cysteine oxidase from Arabidopsis, in the presence of O_2 (Fig. 1*B*). Therefore, DLOR serves as a ratiometric reporter of Cys-NDP activity in yeast. As cognate cysteine oxidase, we chose AtPCO4, the most catalytically potent PCO isoform and fastest to trigger DLOR stabilization upon enzymatic inhibition (5, 38).

We thus probed the double mutant with the proteasome inhibitor MG132 to ascertain cell permeability to this chemical agent. To infer the inhibition of proteasome activity, we measured the expression of two marker genes, *Hexose Transporter 11* (*HXT11*) and *Succinate Dehydrogenase 9* (*SDH9*), known to be synergistically regulated by the proteasome and the TOR (Target of rapamycin) pathway (50). The double mutant displayed a stronger MG132 response than the single *pdr5Δ* and *erg6Δ* mutants, which in turn showed comparable inductions to each other, whereas in the corresponding wild-type strain BY4742 the marker genes were unaffected by the treatment (Fig. S1*B*). Growth of wild-type cells was not affected by MG132, whereas the single and, more evidently, double mutant strains showed significantly decreased OD_{600} values upon treatment (Fig. S1*C*).

Co-transformation of the mutants with DLOR and AtPCO4 showed that in *pdr5Δ* and the double mutant $RAP2.12_{2\text{-}28}$ stability increased in response to MG132, to a similar extent, but not in BY4742 or *erg6Δ* (Fig. S1*D*). Overall, the data suggest that the *pdr5Δ,erg6Δ* strain had significantly higher chemosensitivity than BY4742 or single mutants.

Aiming at a compatible set-up for large-scale experiments with broad panels of compounds, we tested the adaptability of the reporter output to a microtiter plate format of growth. The adoption of microculture formats is also desirable in terms of affordability of chemical screening, as it would make it possible to apply reduced amounts of compounds. Cultures of the double mutant strain were scaled down from 5 ml volume, hosted in individual tubes, to 200 µl in 96-well plates. When DLOR output was compared in the two set-ups, no differences could be detected either in the basal level of activity under control conditions or upon reporter stabilization with MG132 (Fig. S1*E*). This suggests that proper oxygen diffusion in the microculture could be ensured in our set-up, enabling the destabilization of the substrate under control conditions, and that the normalized DLOR output was unaffected by the downscaling. Collectively, these tests indicated that a synthetic strain co-expressing DLOR and AtPCO4 in the *pdr5Δ,erg6Δ* background, hereafter indicated as $syNDP_{\Delta\Delta}$ strain (Fig. 1*B*), is a suitable heterologous platform for the evaluation of chemical effectors of the plant cysteine N-degron pathway in large-scale experiments.

Survey of a chemical compound library with the yeast Cys-NDP reporter platform

We used the $syNDP_{\Delta\Delta}$ strain to carry out a high-throughput screening (HTS) on a small molecule collection, the Natural Product-Like library (Fig. 1*B*, Table S1) (51). This contains a broad range of synthetic compounds characterized by structural similarity to natural compound scaffolds. Minimum size of the collection is ensured through the application of a rational design aimed at avoiding structural redundancy.

To carry out the HTS in the microtiter plate format, 200 µl pre-grown $syNDP_{\Delta\Delta}$ cultures were treated in individual wells with 1 µl of stock compound solution, corresponding to a 50 µM treatment dose, and incubated for 6 h (Fig. 1*C*). The outcome of the screening was expressed as DLOR reporter activity in each well (Fluc/Rluc ratio), normalized over the basal activity of the reporter in DMSO-treated cells to calculate a fold change of output. A proteasome inhibitor treatment with 50 µM MG132 was included in every plate (Fig. 1, *C* and *D*) to provide a positive control during the screening procedure and also enable us to set a threshold for chemical Cys-NDP inhibition.

We first evaluated potential toxicity issues associated with the molecules under testing, since some chemicals might affect the DLOR output due to repression of cell growth, rather than through specific inhibition of the Cys-NDP. In fact, the protein synthesis inhibitor cycloheximide (CHX) that we included in the set-up as a toxic compound (52), made us aware of potential artifacts arising from exclusively relying on the calculated DLOR activity. The addition of CHX at 50 µM dose, albeit leading to high DLOR activity (1.5- to 47-fold higher activity than mock treatment; Fig. S2), was associated with low absolute luciferase signals, arising from poor cell survival. To overcome this limitation of the reporter assay, the luminescence output was complemented with growth data, taking the generation time as the most informative parameter summarizing growth dynamics (Fig. S3). Lethality could now be spotted from an increased generation time, due to flattening of the growth curve in the microculture (Fig. 1*E*, 1G9 and CHX treatments). We observed widespread harmful effects across the collection, with many compounds hindering or abolishing yeast replication (Figs. S3 and 1*F*).

We then proceeded to the evaluation of DLOR response to the chemicals. The activity of the reporter in control conditions was consistent across the 16 plates processed in the screening, with a basal Fluc/Rluc ratio of 0.065 ± 0.015 (n = 16) in DMSO-treated cells (Tables S1 and S2), comparable with previous tests (Fig. S1*E*). The reproducibility of the output in basal conditions further supports the validity of the screening platform. In the subsequent selection step, molecules able to stimulate DLOR stabilization by at least 60% of the extent promoted by MG132 were maintained as Cys-NDP inhibitor candidates. Stabilization by MG132 ranged from 1.20 to 4.55 fold, with an average value of 2.80 ± 0.39 (n = 16; Table S2, Fig. S2). More than half of the tested molecules did not appear to inhibit the N-degron pathway and instead led to mild (between 0.5 and 1 fold change, 603 compounds) or strong (<0.5 fold change, 64 compounds) destabilization of the reporter (Fig. S2). Their effects, potentially connected to enhanced Cys-NDP activity or to some pathway-independent regulation, were not further investigated in this study. In contrast, 45 compounds promoted DLOR stabilization, overcoming the

ASBMB

arbitrary threshold of 60% of MG132 effect on their respective plates (Fig. S2 and Table S3).

Although, the generation time of mock-treated cultures suggested the existence of some technical variability across plates, the ratiometric nature of the DLOR is expected to compensate for growth differences, provided that cultures are equally exponentially replicating. The output of the reporter screening was consequently filtered based on yeast generation time. Among the 45 molecules that had been associated with potential inhibition of the N-degron pathway, this analysis highlighted 26 candidates with very mild to mild negative effect on cell replication (normal growth rate no more than halved) and therefore negligible cytotoxicity (Table S3).

Dissection of the sensitivity of the Cys-NDP enzymes to a subset of target compounds

Our main goal was to identify inhibitors of AtPCO4, out of the candidates extracted through the screening procedure. We thus focused on putative non-cytotoxic inhibitors and analyzed their effect on the individual steps that compose the Cys-NDP. To this end, we expressed the Cys2-substituted DLOR versions D-DLOR and R-DLOR in the *pdr5Δ,erg6Δ* background, to compare them with the original (C-)DLOR reporter. While (C-)DLOR requires oxidation by AtPCO4 to enter the degradation pathway, Cys2Asp substitution in D-DLOR provides a direct target for arginylation by endogenous ATE1 (Fig. 2*A*); therefore D-DLOR stability will increase upon inhibition of ATE1, UBR1, or the proteasome but not AtPCO4. A Cys2Arg substituted reporter (R-DLOR) can instead be directly polyubiquitinated (Fig. 2*A*) and will thus only be sensitive to UBR1 or proteasome effectors. According to this strategy, *bona fide* PCO inhibitors are then expected to hamper C-DLOR degradation without affecting the other Cys2-substituted substrates of the N-degron pathway.

Twenty out of 26 selected molecules could be successfully re-tested (Fig. 2*B* and Table S4). Nine of them—1A7, 1C2, 1E4, 2A2, 2A10, 3B4, 3H9, 4C5 and 4D5—exerted a stabilizing effect on C-DLOR beyond the threshold set at this stage (1.5 fold Fluc/Rluc change over DMSO). Two among those (1E4, 2A2) also promoted significant D-DLOR stabilization beyond the threshold without affecting R-DLOR, which identifies them as potential ATE inhibitors. Molecule 8B7 stabilized equally the three DLOR versions, however low Fluc and Rluc values associated with this treatment suggested a general impairment of protein synthesis, rather than a specific effect on the N-degron pathway. Excluding 8B7, none of the molecules increased R-DLOR output, suggesting the absence of UBR1

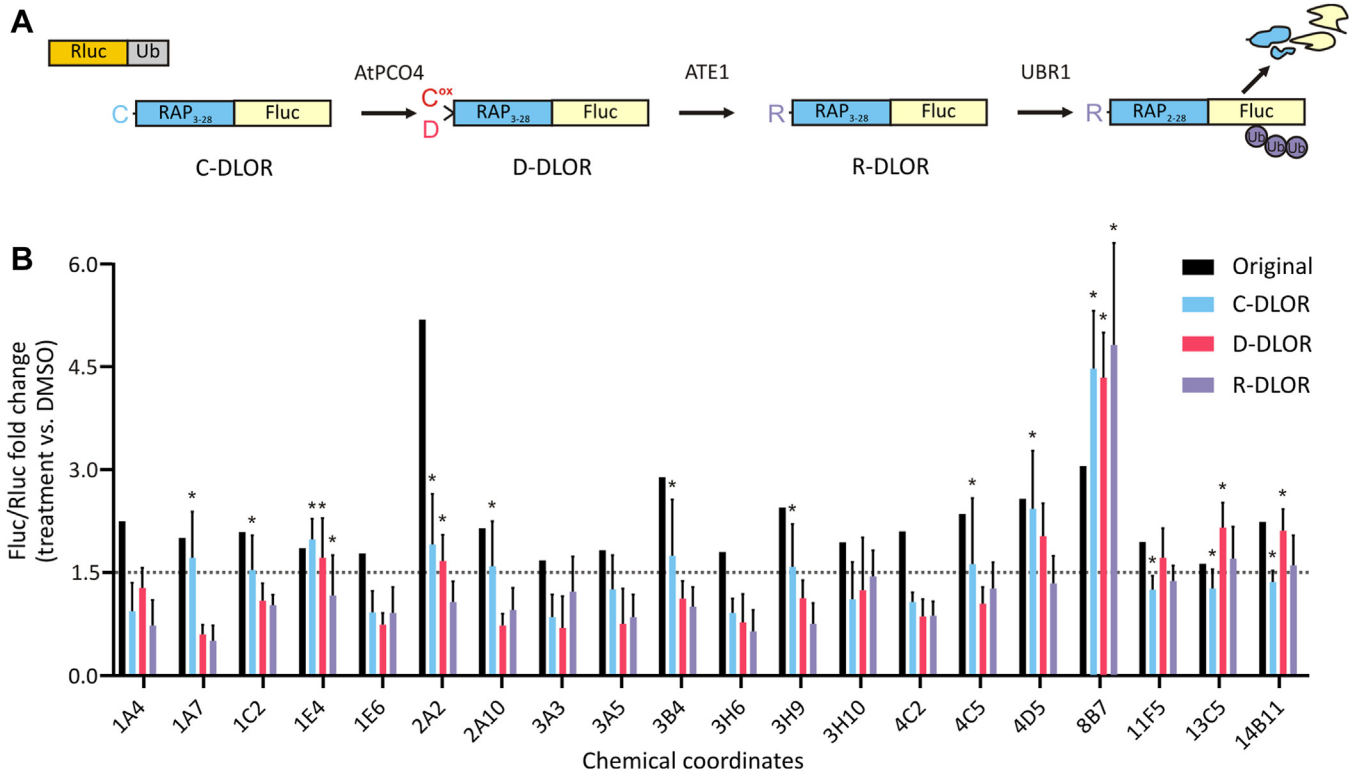

Figure 2. Dissecting the action of Cys-NDP inhibitors on the components of the pathway with yeast DLOR reporters. *A*, fate of C-, D- and R-DLOR reporters according to Cys-NDP dependent regulation. ATE1 and UBR1 are endogenous Arginyl-tRNA-protein transferase 1 and E3 ubiquitin-protein ligase, respectively, composing the yeast Arg-NDP. *B*, effect of the selected compounds from Table S3 DLOR stability. Cells were treated with 50 μM of each compound (1/200 dilution in the microcultures) or 0.5% DMSO (v/v) for 6 h, as in the previous screening. Histograms are mean + SD (n = 4) of the fold change of DLOR activity (Fluc/Rluc) over the relative DMSO control treatment. The reference value from the previous screening is reported as a black column for each compound. The *dashed line* indicates the arbitrary threshold (fold change = 1.5 over DMSO) chosen for substrate stabilization at this stage. Fold change values can be found in Table S4. Two-tailed Student's *t* test (n = 4) was performed on the treatments that induced DLOR stabilization; *asterisks* represent significantly higher Fluc/Rluc ratios for each DLOR version over their respective DMSO controls (two-stage linear step-up procedure of Benjamini, Krieger and Yekutieli, with Q = 1%); $p < 0.05$.

inhibitors or proteasome inhibitors from the panel. Finally, no molecules from this subset affected the stability of D-DLOR or R-DLOR alone, in line with the assumption that these substrates are specifically regulated through the Cys-NDP pathway, whose steps work in a sequential fashion.

Overall, the heterologous portion of the PCOff pipeline set up in *S. cerevisiae* enabled us to shortlist six *bona fide* AtPCO4 inhibitors and two ATE inhibitors from the natural product-like collection with no harmful influence on general protein synthesis or cell viability, amenable to the subsequent assays in plants (Table S4).

Effect of candidate Cys-NDP inhibiting molecules on ERF-VII activity in plants

To assess the efficacy in plants of the hits selected from the yeast screening, we took advantage of a stable transgenic line of *A. thaliana* expressing a *35S:RAP2.12*$_{1\text{-}28}$*-Fluc* reporter construct (7). In this 28RAPFluc line, firefly luciferase activity is a proxy of the proteolysis triggered by PCO through the Cys-NDP, similar to the DLOR in yeast.

We first tested the responsivity of the 28RAPFluc reporter to chemical impairment of the proteasome after intervention with MG132 or bortezomib (BZ), known to be more effective in blocking the proteasome than MG132 in Arabidopsis (53). Both inhibitors were able to raise the signal of the 28RAPFluc reporter in 5-day-old seedlings, with a stronger effect at 1 mM dose than at 100 μM (Fig. S4*A*). However, 1 mM BZ caused visible phenotypic effects on seedlings, which appeared slightly bleached in comparison with mock- or 100 μM BZ treatments (Fig. S4*B*). Therefore, in order to minimize any potential chemical toxicity, we opted for maintaining 100 μM as the positive control dose in the forthcoming plant experiments and selected BZ as the most effective proteasome inhibitor in stabilizing the reporter at the selected dose. Similarly, a 100 μM dose of each tested compound was applied to plants, which also allowed us to maintain the same range of chemicals as the one used in the yeast-based screening (50 μM).

We subsequently examined the response of seedlings to any shortlisted Cys-NDP inhibitor from Table S4 available from stock (seven compounds, all identified as putative PCO inhibitors in yeast). After 6 h application, five of them stimulated 28RAPFluc activity by at least twofolds (Fig. 3*A*): 1C2, 2A10, 3H9, 4C5 and 4D5. Two additional compounds from the screening were included as controls: 9B6, which had displayed adverse effects on yeast growth, and 8B7, which affected protein regulation. Neither of them was able to modulate 28RAPFluc abundance (Fig. 3*A*), suggesting that their mode of action may not be compatible with plant cells but rather be yeast cell-specific. Strong inhibition of the pathway was, instead, achieved with the application of 100 μM BZ, which consistently elicited over 60-fold increase in the stability of the reporter.

Stabilization of the ERF-VII factors in aerobic tissues is expected to enable more prompt responses if low oxygen conditions set in. This is in turn expected to be reflected by better stress tolerance. Therefore, the five chemicals that had proven able to restrain 28RAPFluc degradation (identities and structures in Table S5) were used to prime wild-type Arabidopsis seedlings against anoxia. 50 μl of a stock solution (100 μM) of each compound was supplied to seedlings growing individually in microtiter wells, in order to soak the agarized medium without submerging the aerial tissues. Six hours after the chemical treatment, seedlings were subjected to 15 h dark anoxia, expected to impose harsh stress on unprimed wild-type seedlings (54). Accordingly, DMSO-treated plants survived anoxia but displayed considerable chlorophyll loss and stunted growth (Fig. 3*B*). No improvement could be achieved with two chemical treatments (1C2 and 3H9) however three other compounds strikingly enhanced seedling performance under stress: full pigment recovery and minor growth penalties were associated with 2A10, 4C5, and 4D5 pre-treatments, suggesting that these molecules may be effective in priming the anaerobic response (Fig. 3*B*). BZ application led, instead, to complete mortality, indicating that indiscriminate proteasome inhibition is not a viable strategy to promote hypoxia tolerance *via* down-regulation of the Cys-NDP.

We speculate that the observed improvements in stress tolerance were a consequence of stimulated anaerobic gene expression in response to chemical treatments. To investigate this, we first tested the anaerobic gene response to the treatment by means of the reporter line *promADH:GUS* (55), where the β-glucuronidase gene is expressed under the control of the hypoxic promoter *ADH1* (*Alcohol Dehydrogenase 1*). All five compounds were able to activate the promoter to some extent, in both roots and emerging leaves, and, in the case of 2A10 and 3H9, the induction appeared to be stronger than the one observed after an equal duration under hypoxia or BZ (Fig. 3*C*). To characterize the low oxygen response of treated plants further, we measured the expression of nine core anaerobic genes (56) in wild-type seedlings, restricting the analysis to those chemicals that ameliorated stress tolerance. After 6 h of chemical treatment, changes could be observed in the steady state level of six anaerobic transcripts, *ADH1*, *Hypoxia Responsive ERF 2 (HRE2), Pyruvate Decarboxylase 1* (*PDC1*), *Phytoglobin 1* (*PGB1*), *Hypoxic Response Attenuator 1* (*HRA1*), *Acyl Carrier Protein Desaturase 6* (*SAD6*) *Lateral organ Binding Domain 41* (*LBD41*) and *Plant Cysteine Oxidase 1* (*PCO1*) (Figs. 3*D* and S4*C*). Molecule 2A10 elicited again the strongest response, followed by 4C5, while 4D5 had undetectable effects on gene expression, at the time point evaluated (6 h). Chemical or hypoxic treatments did not alter the expression of *RAP2.12*, *RAP2.2*, and *RAP2.3*, confirming that an exclusive posttranscriptional regulation of the hypoxic sensing machinery was taking place (Fig. S4*D*). The ROS stress markers *Respiratory Burst Oxidase Homolog Protein D* (*RBOHD*) and *Ascorbate Peroxidase 1* (*APX1*) remained unchanged, suggesting that general stress responses were not invoked by the treatments. Moreover, the induction of the iron deficiency marker *Ironman 1* (*IMA1*) (57) by 4D5 hints at a possible PCO inhibitory effect by this chemical through iron chelation (Fig. S4*D*).

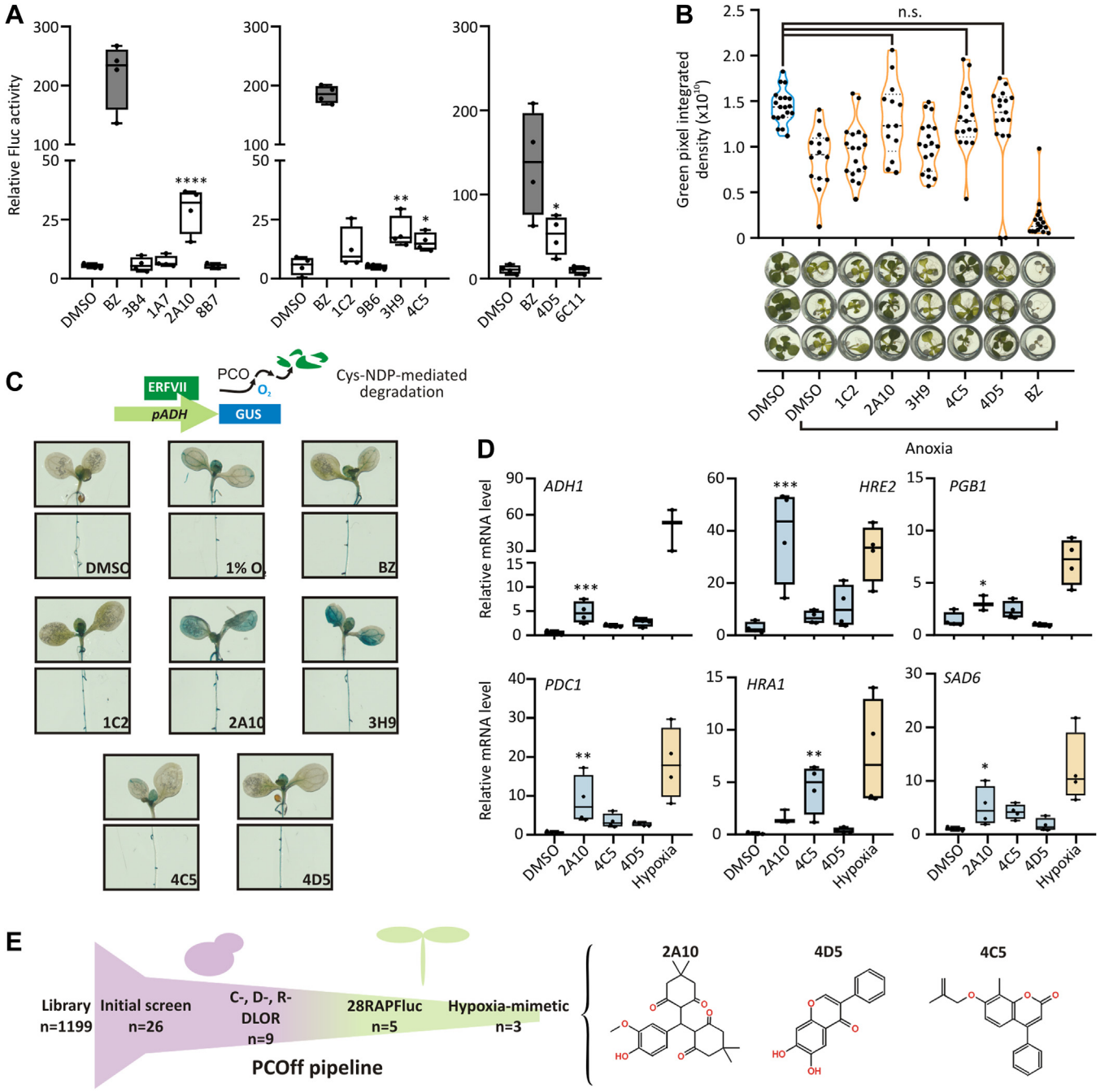

Figure 3. Impact of candidate Cys-NDP inhibiting compounds from the chemical screening on the 28RAPFluc reporter of Arabidopsis. *A*, luciferase activity (Fluc μg^{-1} protein) after 6 h application of 100 μM chemicals or 1% v/v DMSO on 5-day-old seedlings grown in liquid media. Data are mean ± SD (n = 4). *B*, impact of 15 h-long dark anoxia on 7-day-old seedlings pre-treated with 50 μl of 1% DMSO (v/v) or 100 μM chemicals. Chemical treatments were administered 6 h before the stress. Better tolerance was indicated by higher chlorophyll levels at the end of a 6-day-long recovery period, digitally estimated from a higher density of *green* pixels in the shoot image area. Some DMSO-treated plants were kept unstressed (*blue* violin plot) for comparison. Individual and median values are shown for each treatment (n = 14–20). *C*, histochemical β-glucuronidase (GUS) assay on *promADH:GUS* (55) reporter plants (7 day-old, grown in vertical plates) treated with 100 μM of the indicated chemicals, 1% DMSO in normoxia or 1% DMSO in hypoxia (1% O_2 v/v) for 6 h. *D*, expression of six hypoxia-inducible marker genes in wild-type seedlings treated as in (*C*). *E*, overview of the PCOff pipeline and number of chemicals analyzed (n) that overcame each threshold in yeast (lilac) and plants (*green*), together with the 2-D structures of 2A10, 4D5, and 4C5, identified as possible hypoxia mimetic molecules, retrieved from their catalog numbers (Table S1) at Otava Chemicals. Box plots represent the median (line) and interquartile range (IQR), whiskers span from minimum to maximum values (n = 4). Statistical significance was determined with a one-way ANOVA followed by a Dunnett's multiple comparison tests on relative Fluc activity (*A*, BZ treatment excluded), *green* pixel density (*B*) and relative mRNA level (*D*, hypoxic treatment excluded) (****$p < 0.0001$; ***, $0.0001 \le p < 0.001$; *, $0.01 \le p < 0.05$). BZ, bortezomib.

The above evidence indicates that some of the compounds selected from the heterologous assay could also be taken up by Arabidopsis seedlings, hinder ERF-VII degradation (Fig. 3*A*), and activate the anaerobic promoters in normoxia after short-term treatment (Fig. 3, *C* and *D*), with 2A10 being consistently the most effective one. The efficacy of the compounds at alleviating the impact of sublethal anoxia, instead, appeared to be modulated by additional factors, which neutralized 3H9

priming potential and, in contrast, reinforced the effect of 4D5 and 4C5 (Fig. 3*B*). In summary, among the 1199 chemicals analyzed in the PCOff pipeline (Fig. 3*E*), we identified 26 potential pathway inhibitors in yeast that did not alter cell growth or protein homeostasis and nine short-listed compounds as specific AtPCO4 or ATE1 inhibitors. Five were confirmed to increase the stability of the ERF-VII reporter 28RAPFluc. Three of them, once applied to Arabidopsis seedlings, coherently elicited the expression of hypoxia marker genes and plant survival under anoxia, qualifying as hypoxia-mimetic molecules in plants. Inspection of the structures of these three molecules (Fig. 3*E*, Table S5) revealed that 4C5 belongs to neoflavones (4-phenylcoumarin derivatives), 4D5 is similar to isoflavones (3-phenylchromenone derivatives) and 2A10 is a substituted bis-cyclohexanedione compound. When compared to other deposited structures, 2A10 only showed significant resemblance to synthetic molecules, but not to natural products, whereas 4D5 and 4C5 resembled several natural cumarins and neoflavones, or isoflavones, respectively.

Effect of candidate Cys-NDP inhibiting molecules on the activity of recombinant AtPCO4

The natural product-like library from which the compounds were identified comprised a broad range of chemical structures with the potential to modulate diverse cellular processes. To confirm that the observed effects in seedlings were due to direct inhibition of PCO activity, we therefore determined the impact of the five identified candidates on the activity of recombinant AtPCO4 (the most active of the five AtPCOs (5)). Following preincubation of the enzyme with compound at 1 mM or solvent-only control, 0.5 μM AtPCO4 was incubated with 500 μM 16-mer peptide representing the Cys-initiating N-terminus of RAP2.12 ($RAP2_{2\text{-}17}$) for 10 min under standard assay conditions (5). The activity of AtPCO4 in the presence of each inhibitor was compared to equivalent assays in the presence of solvent-only controls and revealed that activity was significantly reduced in the presence of 2A10 and 4D5 (Fig. 4*A*). Further analyses revealed that both 2A10 and 4D5 inhibited AtPCO4 activity in a concentration-dependent manner, with IC_{50} values determined to be 264.4 ± 1.07 μM and 349.6 ± 1.2 μM, respectively (Fig. 4, *B* and *C*). This strongly indicates that the effects observed in the *in vivo* experiments are indeed caused by direct PCO inhibition.

We attempted to generate crystals of AtPCO4-2A10 complexes in order to visualize 2A10 binding to AtPCO4; however, this was unsuccessful, possibly related to the relatively high IC_{50} value and therefore likely weak binding affinity. We therefore used AutoDock Vina (58, 59) molecular docking software to predict potential 2A10 binding sites on the

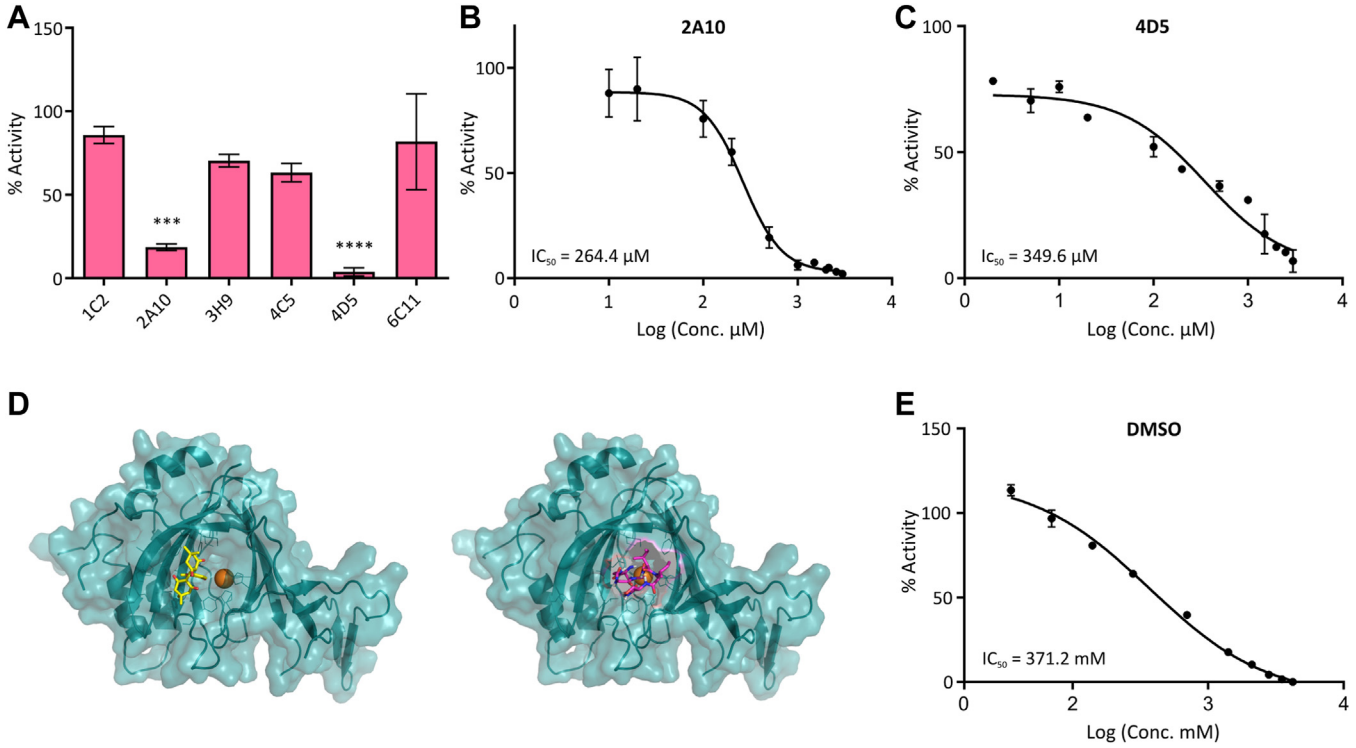

Figure 4. Inhibition of recombinant AtPCO4 activity by Cys-NDP inhibiting compounds. *A*, effect of 5 candidate Cys-NDP inhibiting compounds on AtPCO4 activity towards a peptide representing Nt-Cys initiating RAP2.12 ($RAP_{2\text{-}17}$ herein) relative to DMSO controls. $RAP_{2\text{-}17}$ (500 μM) was reacted with AtPCO4 (0.5 μM) pre-incubated with 1 mM inhibitor or DMSO vehicle only, for 10 min at 25 °C. A non-hit molecule from the screening (6C11) was included as a negative control. Data represent mean ± SD (n = 3), statistical significance determined comparing AtPCO4 activity co-incubated with each candidate compound compared with the negative control, by one-way ANOVA followed by a Dunnett's multiple comparison test (****$p < 0.0001$; ***, $0.0001 \le p < 0.001$). *B* and *C*, dose-response curves for 2A10 (*B*) and 4D5 (*C*) treatment of AtPCO4 activity; reactions were performed as described for (*A*) with inhibitor present at concentrations indicated by the logarithmic scale. Data are presented as mean ± SD (n = 3). *D*, autodock modeled structures of AtPCO4 (PDB 6S7E) (*teal*) in complex with 2A10 (*yellow sticks*, *left*) and $RAP_{2\text{-}8}$ (*pink sticks*, *right*). Both occupy the putative substrate binding site. Metal at the active site is shown by an *orange sphere*; AtPCO4 residues which line the active/substrate binding site are shown with *teal lines*. *E*, dose–response curves for AtPCO4 activity in the presence of increasing concentrations of DMSO, indicated by the logarithmic scale. Data are presented as mean ± SD (n = 3).

AtPCO4 structure (Fig. S5*A*). The lowest energy conformation (−7.7 kcal/mol, Fig. S5*B*) suggested favorable binding of 2A10 in the substrate-binding pocket of AtPCO4 (Fig. 4*D*, 2A10 in yellow). Although local conformation in the active site is likely to change upon ligand binding and the docking was performed against a static AtPCO4 structure, this does suggest that 2A10 may compete with substrate for binding at the active site. This is supported by an AutoDock4 (60) modeled structure of a 7-mer peptide representing Nt-Cys initiating RAP2.12 ($RAP2_{2\text{-}8}$) bound in the same substrate-binding pocket (Fig. 4*D*, $RAP2_{2\text{-}8}$ in pink; Fig. S5, *C* and *D*).

Both 2A10 and 4D5 were solubilized in DMSO, and therefore inhibition was determined by comparison to DMSO-only controls. In the course of conducting these controls, we noticed that DMSO was also having an inhibitory effect on AtPCO4 activity (Fig. 4*E*); DMSO-mediated inhibition has also been observed in other enzyme systems (61, 62), with non-specific inhibitory effects rationalized through hydrogen-bonding with catalytic residues or general effects on solubility (61). The IC_{50} value for AtPCO4 DMSO inhibition (371.2 mM) was high compared to the potencies of the inhibitors used in this study; however, this corresponds to a DMSO v/v concentration of 2.64%. Given that DMSO is a common solvent for chemical compound libraries, the presence of DMSO at even 1% could result in a 20% reduction in AtPCO4 activity. DMSO-mediated effects on enzyme stability and solubility will likely differ in *in vivo* and *in vitro* environments. When evaluated on plants, DMSO treatments between 1 and 5% only led to a slight upregulation of *ADH1* and *PCO1* (Fig. S6). Nevertheless, the potential for DMSO solvent to impact AtPCO activity should be considered in future screens for potential inhibitors.

We finally tested the effect of 2A10, the most promising inhibitor of AtPCO4, in the human homologue of the enzyme, HsADO. Both enzymes share sequence and overall structural homology (17, 28, 63–65). RGS4 represents an established substrate of ADO, the human Regulator of G-protein Signaling (30). Interestingly, 2A10 was not able to alter ADO activity toward an RGS4 substituted version of the DLOR (Fig. S7*A*), nor decrease its activity *in vitro* (Fig. S7*B*), suggesting that subtle differences in active site structure may facilitate specific binding of 2A10 to AtPCO4.

Discussion

Promoting or improving plant hypoxic responses may ameliorate crop production losses due to flooding events (66), and the manipulation of plant sensitivity to oxygen is a conceivable strategy to protect them against low-oxygen-associated environmental stresses. In this study, we designed a heterologous strategy to assist the identification of chemical compounds able to interfere with the dedicated oxygen sensing pathway from plants, the cysteine N-degron pathway (Cys-NDP). Different from the case of the human HIF-VHL pathway, which has been extensively probed for sensitivity towards chemical inhibitors, no attempts for the pharmacological modulation of oxygen sensing have been made in plants yet. Time-restrained application of agrochemical formulations of Cys-NDP inhibitors may simulate hypoxic conditions in plants and invoke priming responses that can help plants withstand subsequent flooding events (67, 68).

The Cys-NDP couples a step committed to direct oxygen perception, performed by PCO enzymes, with a more general proteolytic pathway (7, 10), therefore the modulation of PCO activity is expected to be key to achieving specific control on oxygen sensing. PCOs can be targeted through genetic approaches that include site-directed mutagenesis towards less active enzyme variants, or multiple knock-outs to overcome functional redundancy of the different PCO isoforms of Arabidopsis (28, 34). Nonetheless, constitutive impairment of the Cys-NDP cannot be uncoupled from a severe fitness reduction (34), a drawback that may be overcome with a chemical strategy for the transient control of PCO activity. Here, we identified and characterized three small molecule inhibitors of PCO in Arabidopsis, which qualify as the first described hypoxia-mimetic molecules effective in plants (Fig. 3). Two of them could be confirmed as *bona fide* PCO inhibitors through biochemical assays, with IC_{50} values of 264 μM for 2A10 and 350 μM for 4D5 towards AtPCO4 (Fig. 4).

The hypoxia mimetic candidates discovered here belong to a large panel of small molecules of synthetic origin, but bearing structural resemblance to natural products. Synthetic hybrids of natural scaffolds introduce variations in their functional groups, aiming to maintain a backbone structure similar to those evolved in nature (69). This biased method has been applied to increase the variability of functional structures, for the discovery of new cancer therapies, herbicides, and antibiotics (70, 71). With the lack of any pre-existing knowledge of PCO-inhibiting molecules, we opted for an unbiased full library screening. The synthetic hydrocarbons included in the Natural Product-Like collection we surveyed have been computationally selected to avoid structural redundancy; this strategy enables maximizing the structural diversity of natural scaffolds, which constitute an ideal source of bioactive molecules for drug discovery while reducing the complexity of the *in vivo* screening (72, 73). The same library used in this study has been previously exploited to identify inhibitors targeting bacterial efflux pumps in the human pathogen *Pseudomonas aeruginosa* and to determine that auxin regulates bacterial antibiotics production (51, 74).

The core idea in our chemical survey was the adoption of budding yeast as a convenient *in vivo* platform for the evaluation of candidate effectors of the Cys-NDP for the subsequent application to plants. The platform is based on a synthetic yeast strain ($syNDP_{\Delta\Delta}$) where an orthogonal Cys-NDP was implemented, leveraging the lack of cysteine dioxygenases and ERF-VII substrates in yeast (5, 38). Yeast-based approaches exploiting yeast orthogonality have been applied (mainly assaying growth as primary output) to find inhibitors of animal cellular processes (75–77). Fewer yeast-based chemical screenings targeting plant processes have been instead undertaken to date, among which the identification of jasmonate signaling inhibitors through a yeast-two-hybrid growth assay (35). In our pipeline, insulation of the DLOR-AtPCO4 module

from yeast regulatory pathways minimized the possibility of indirect interactions between the chemicals and the Cys-NDP. Interference of known regulators of ERF-VII stability, such as NO (78, 79) or ethylene (which is not produced by yeast) (80), could be ruled out as well. In fact, NO interacts with the pathway at a yet unknown level, without affecting Cys2 oxidation (81), but has proven ineffective on the synthetic Cys-NDP of yeast (38).

The choice of yeast over plants as the initial testing platform of the pipeline guaranteed a high-throughput set-up, similar to other screenings based on *S. cerevisiae* (77, 82), in which a large number of molecules and a minimal compound volume could be easily handled. Additionally, yeast enabled easy assessment of cell growth rate in the presence of the treatments and its subsequent use as a secondary output of the screening, to filter out those compounds likely to affect reporter output indirectly, through the impairment of growth-related cellular processes (83, 84). Nearly half of the chemicals from the library indeed impacted growth, either by inhibiting or by promoting it over DMSO-treated samples (Fig. S3). Although extraneous to our goal, this large set of molecules might still encompass interesting candidates with antifungal or growth-promoting properties, as demonstrated by previous screenings adopted to search for new fungicides (85). Beyond revealing potential modulators of yeast growth, this assessment granted robustness to the luminescent output of the screening, which is a reliable proxy of Cys-NDP activity in actively growing cultures.

We adapted our screening strategy to overcome yeast resilience towards xenobiotic stresses, by introduction of the synthetic Cys-NDP reporter circuitry into a chemosensitive genotype generated on purpose. Although widely used as a platform for drug discovery studies (36, 37), yeast is characterized by poor sensitivity to exogenous chemicals, due to extensive detoxification mechanisms based on Pdr5p and other ABC transporters and low membrane permeability (86–88). The wild-type background BY4742 indeed became chemically sensitive only after ablation of *PDR5* and the key ergosterol biosynthesis gene *ERG6* (Fig. S1). Similarly, a *pdr5Δ,erg6Δ* strain described previously, YNK591, shows a higher intake of lipophilic and DMSO-based drugs (43). It has been suggested that cells lacking Pdr5p may be more vulnerable to exogenous chemicals than those lacking Erg6p (89), but both act synergistically and make a double *pdr5Δ,erg6Δ* mutant a better candidate for chemical screenings (46). The $syNDP_{\Delta\Delta}$ strain thus allowed us to minimize the dose of applied chemical needed to exert an effect in the screening phase. Nevertheless, lower intake capacity by Arabidopsis plants cannot be excluded and may explain the inefficacy of some positive hits released in this phase in the following step of the pipeline (Fig. 3).

The PCOff pipeline allowed the effective identification of three direct inhibitors of the Cys-NDP and the dissection of their effect on the steps of the pathway (Fig. 3). The modular nature of the synthetic strategy on which the $syNDP_{\Delta\Delta}$ strain is based makes it possible to test Cys2-substituted variants of the substrate as well as heterologous Cys-NDP components (90). Here, we proved the adaptability of the yeast platform to the human ADO-RGS4 module (Fig. S7*A*). The modularity of the platform offers a straightforward strategy to survey specific effectors of the downstream components of the pathway. Ubiquitin-fusion model substrates have been indeed already deployed to identify small molecule inhibitors of UBR1 type N-recognins (91–93).

Among the three inhibitors validated in Arabidopsis, the neoflavone 4C5 and the isoflavone 4D5 are phenyl derivatives of coumarin or its isomer chromone, respectively. A large number of natural neo- and isoflavones have been associated with antioxidant, anti-microbial, anti-inflammatory, anti-cancer, or hormone-like properties, related to the wide diversification of functional groups of these natural scaffolds, with a few therapeutic candidates (94–96). The iron deficiency marker *IMA1* indicated that 2A10 and 4C5 are unlikely to work through Fe^{2+} chelation, while 4D5 may interact with iron availability in Arabidopsis (Fig. S4). 2A10 is a phenyl-substituted bis-dimedone derivative. Dimedone (5,5-dimethyl-1,3-cyclohexanedione) can react with Cys-sulfenic acid moieties, generated from the oxidation of reactive thiols (97). Although this may suggest a reactivity of 2A10 with Cys2 residues in MC- substrates, the kinetic data and the lack of inhibition of 2A10 on HsADO (Fig. S6) rather indicate an interaction between the molecule and PCOs. Docking experiments predicted it with AtPCO4 catalytic site, in the vicinity of the RAP2.12-binding pocket (Fig. 4). According to this simulation, 2A10 specificity towards AtPCO4 may be related to the structural diversity between ADO and PCO catalytic sites (63).

Overall, the drug discovery strategy presented here enabled us to recover the first *bona fide* PCO inhibitors found to date with the potential to induce hypoxic responses in plants. This initial identification of PCO inhibitors and the predictive modeling of their interaction with AtPCO4 pave the way for the structure-guided optimization of the small molecules found here towards enhanced bioactivity and target specificity.

Experimental procedures

Plant material

Col-0 wild-type plants were used as reference ecotype. The *A. thaliana* transgenic lines used, 28RAPFluc (*p35S:RAP2.12$_{1-28}$-FLUC*) (7) and *promADH:GUS* (55), have been described previously. In all axenic experiments, seeds were sterilized by thoroughly mixing with 70% ethanol followed by 10% (v/v) bleach, then rinsed with sterile water for six times and vernalized in the dark for 2 days at 4 °C before sowing. Seedlings were grown at 22 °C day/18 °C night under neutral photoperiod (12 h light) with 150 μmol m^{-2} s^{-1} photon flux density, on half-strength MS medium (Duchefa) supplemented with 1% (w/v) sucrose. To assess reporter activity, 28RAPFluc seeds were germinated in wells of 48-well polystyrene plates containing 500 μl of liquid medium and sampled after 5 days. *PromADH:GUS* and wild-type seeds were sown on vertical square plates supplemented with 0.9% agar, and grown for 7 days prior to chemical treatments. For anoxia survival, Col-0 seeds were germinated individually in microtiter plate

wells on 100 µl medium supplemented with 0.5% agar and grown for 7 days before treatments.

Yeast strains

The *S. cerevisiae* mutant strains *erg6Δ* (*Matα; his3-Δ1; leu2-Δ0; lys2-Δ0; ura3-Δ0; YML008C::kanMX4*) and *pdr5Δ* (*Matα; his3-Δ1; leu2-Δ0; lys2-Δ0; ura3-Δ0; YOR153w::kanMX4*) were purchased from Scientific Research and Development GmbH, along with their haploid parental strain BY4742 (*Matα; his3-Δ1; leu2-Δ0; lys2-Δ0; ura3-Δ0*), used as wild-type reference.

The *pdr5Δ,erg6Δ* strain was developed from *pdr5Δ* by ablation of the entire *ERG6* coding region (from ATG to TAA) through gene deletion, following the *Delitto Perfetto* approach (47) (Fig. 1*A*). A repair template (ERG6CORE) was generated by amplification of a CORE (COunterselectable marker and REporter gene) cassette from pGSHU (Addgene plasmid #72244) with the primers ERG6CORE_Fw and ERG6CORE_Rv (Table S6), harboring 50 ERG6-specific nucleotides for the homologous recombination. ERG6CORE was amplified with a Phusion proofreading polymerase (Thermo-Fisher Scientific), gel purified, and directly transformed in *pdr5Δ* with the LiAc method. Integration of the cassette was verified by cell selection on synthetic dropout (SD; see "yeast cultivation") without uracil (SD −Ura) and *via* PCR amplification with ERG6Up_Fw/SceI_Rv, obtaining a 400 nt product. Subsequently, ERG6CORE excision was promoted by *SceI* induction in YPGA (20 g L^{-1} peptone, 10 g L^{-1} yeast extract, and 20 g L^{-1} of galactose (Duchefa) supplied with 20 mg L^{-1} adenine hemisulfate (Sigma-Aldrich)) and homology-directed DNA repair was prompted with the ERG6Dis_Fw and ERG6Dis_Rv oligonucleotides (Table S6). Double *pdr5Δ,erg6Δ* mutants were isolated by counterselection on complete SD plates supplemented with 1 g L^{-1} of 5-fluoroorotic acid (5-FOA) and by a concomitant lack of growth on hygromycin-containing YPDA plates (assessed through replica plating). Loss of CORE was further confirmed by PCR, as indicated by a 371 nt product after amplification with the ERG6Up_Fw/ERG6Dw_Rv primer couple and absence of amplification with ERG6Up_Fw/SceI_Rv (Table S6).

Yeast cultivation

Yeast was grown at 30 °C, 150 rpm in liquid SD medium, containing 6.7 g L^{-1} Yeast Nitrogen Base (DIFCO), 1.37 g L^{-1} Yeast Dropout Medium (Sigma-Aldrich) and 20 g L^{-1} glucose, plus supplements (0.16 M uracil, 0.8 M histidine– HCl, 0.8 M leucine and 0.32 M tryptophan (Sigma-Aldrich) when complete), with 20 g L^{-1} agar when solid. Overnight cultures were first diluted to half in fresh media and further diluted to OD_{600} = 0.1 prior to 6 h growth. 5 ml cultures were grown in 35 ml skirted vials, shaking (150 rpm) at 30 °C. 200 µl microcultures were grown at 30 °C in a static regime in U-shaped 96-well plates. Every 2 h, plates were sealed and gently vortexed, prior to OD_{600} measurements, to enhance mixing with the air inside the well.

Untransformed cells were grown on YPDA, containing 20 g L^{-1} peptone, 10 g L^{-1} yeast extract, and 20 g L^{-1} of glucose (Duchefa) supplied with 20 mg L^{-1} adenine hemisulfate (Sigma-Aldrich) and with 20 g L^{-1} agar (Duchefa) when necessary.

Construct preparation and yeast transformation

AtPCO4 and GUS coding sequences were cloned in pENTR-D-TOPO (Thermo Fisher Scientific) and recombined in pAG415GPD (Addgene plasmid #14146), as described in (38). The DLOR (C-DLOR) pENTR plasmid (38) was used as a template for site-directed mutagenesis, to generate the Cys2-substituted versions D-DLOR and R-DLOR. The primers specified in Table S7 (D-DLOR_Fw, D-DLOR_Rv, R-DLOR_Fw, and R-DLOR_Rv) were used to amplify the template with the Phusion proof-reading polymerase (Thermo Fisher Scientific). The reaction products were treated with 20 U of DpnI (Anza, Thermo Fisher Scientific) overnight at 37 °C to degrade the methylated template, and used for direct transformation of competent *E. coli* cells. Each DLOR pENTR version was recombined into pAG413GPD (Addgene plasmid #14142) *via* Gateway LR clonase II mix (Thermo Fisher Scientific). The $RGS4_{2\text{-}22}$ DLOR version (File S1) was synthetically generated, cloned in pENTr-D-TOPO, and recombined into pAG413GPD, as described above. An empty pYES2 (Thermo Fisher Scientific) used to test transformation efficiency on cells plated on SD −Ura.

Yeast was transformed using the LiAc/SS carrier DNA/PEG method (98). Before the transformation, cells were grown overnight in 5 ml and transferred to flasks with 50 ml YPDA or SD −Ura supplemented with galactose (Duchefa), when specified and depending on the strain. Incubation in PEG/LiAc/SS DNA at 42 °C was reduced from 60 to 45 min in the case of the *pdr5Δ,erg6Δ* mutant, to circumvent its sensitivity to the harsh chemical conditions applied during the transformation protocol and obtain a sufficient number of transformed colonies.

Evaluation of yeast growth rates

Microculture cell density was recorded every 2 h after the addition of the chemicals. The OD_{600} was measured in 96-well-growing yeast culture plates using the Multiskan Go 1510 Sky plate reader (Thermo Fisher Scientific) and the values were corrected by means of a calibration curve (99). The following calculated polynomial regression equation of the data was used (R^2 = .9983):

$$y = -8.7202x^2 + 11.363x$$

Generation time (G) was obtained from the corrected OD_{600} values with the following formula (100):

$$G = \frac{tj - ti}{\log_2 10 \times \log_{10} \frac{Ntj}{Nti}}$$

where ti and tj are two subsequent time points (expressed in minutes) and Nt are the corrected OD_{600} values at the same time points. G was calculated over the last two time points of the treatments (4 and 6 h of growth), which in the case of

mock-treated cells fell in the exponential phase across all plates of the screening (Fig. 1*E*, DMSO curve).

Chemical treatments

A set of aliquots from the Natural Product-Like product library from OTAVA Chemicals was arranged in sixteen 96-well plates. The OTAVA Natural Product-Like Library was designed to include synthetic compounds similar to natural products. The compounds were selected by similarity to natural compounds scaffolds and filtered to enhance the chemical heterogeneity. The library contains 1199 compounds such as polyketides, flavonoids, terpenoids, steroids, alkaloids, oxygen heterocycles and coumarins (51). Chemicals were dissolved to 10 mM in 100% DMSO (v/v). MG132, cycloheximide (Sigma-Aldrich) and bortezomib (Merck) stocks were equally dissolved to 10 mM concentration in DMSO.

Yeast cultures from the mutant strain *pdr5Δ,erg6Δ* co-expressing the desired DLOR version and AtPCO4 ($syNDP_{\Delta\Delta}$) were diluted at OD_{600} = 0.1, after which 200 µl suspension per well were dispensed in 96-well plates and treated for 6 h with 1 µl chemicals (50 µM) or DMSO (0.5% v/v), for the mock treatments.

Five- or 7-day-old seedlings (according to what was specified in the main text) were moved to fresh half-strength liquid MS medium containing 100 µM or 1 mM of either the hit compound or bortezomib. Control samples were supplemented with an equal volume of DMSO (1%, 2%, or 10% v/v). Plates were kept shaking (120 rpm) in the dark for 6 h prior to further treatments (anoxia, GUS staining) or sampling by flash freezing in liquid N_2. *promADH:GUS* and wild-type seedlings were grown in vertical square plates in half-strength MS with 0.9% agar and 1% sucrose for 7 days prior to chemical treatment.

The SMILEs of 2A10, 4C5 and 4D5 (Table S5), retrieved from their respective catalog numbers at https://otavachemicals.com, were used as an input for a 2-D structure search of natural analogous products, using the database and online tools available on the website www.coconut.naturalproducts.net.

Low oxygen treatments

Seven-day-old Col-0 seedlings were grown in 96-well plates on half-strength MS (Duchefa) with 1% sucrose and 0.7% agar (Duchefa). Seedlings were pre-treated for 6 h by application of 50 µl solution of the selected chemicals (100 µM) and subsequently moved to anoxic conditions (100% N2 atmosphere), in a Gloveless Anaerobic chamber (COY). Samples were kept at 22 °C in the dark. One plate was kept in the dark under aerobic conditions as control. After 15 h anoxia, plates were moved back to aerobic conditions in the light for 6 days.

For gene expression, Col-0 seedlings grown in vertical square plates on 0.9% agar in half-strength MS and 1% sucrose were moved to liquid media supplemented with 1% (v/v) DMSO and moved to the glovebox equilibrated at 1% O_2 (v/v) in N_2, as described above, for 6 h.

Luciferase measurements

Luciferase activity was quantified from cell lysates using the Dual-Luciferase Reporter (DLR) Assay System (Promega). Yeast cells were recovered by centrifugation and pellets were lysed in 50 µl 1× Passive Lysis Buffer (PLB). Arabidopsis seedlings were ground in liquid N_2 and resuspended in 200 µl PLB. Luciferase activities were measured according to the manufacturer's protocols, using a Lumat LB 9507 Tube Luminometer (Berthold). Luciferase activity values were normalized against the renilla luciferase values for yeast cells containing the ratiometric reporter DLOR (Fluc/Rluc signal ratio), or against the total protein amount (Fluc μg^{-1} protein) in 28RAPFluc plant extracts. Proteins were quantified from plants using the Bradford protein assay (Bio-Rad), following the manufacturer's specifications.

Gene expression analyses

Total RNA was extracted from plants as described by (101). Total RNA was isolated from yeast according to (102), with minor modifications of the protocol. Yeast cells were collected by centrifugation and resuspended in 50 mM sodium acetate, 10 mM EDTA, and 1% SDS. An equal amount of phenol was added to the suspension. Samples were vortexed and incubated at 65 °C for min, then at −20 °C for 15 min, before centrifugation at top speed for 2 min. The supernatant was recovered and subjected to sequential phenol:chloroform:isoamyl alcohol (25:24:1) and chloroform phase extraction. Finally, nucleic acids were precipitated by centrifugation from the aqueous phase, using two volumes of ice-cold absolute ethanol supplemented with sodium acetate at a final concentration of 300 mM. RNA pellets were resuspended in RNAse-free water.

One µg total RNA was processed to cDNA with the Maxima cDNA synthesis kit (Thermo Fisher Scientific), according to the manufacturer's protocol. Gene expression levels were assessed by Real-time qPCR according to Bui *et al.* (103), with an ABI Prism 7300 sequence detection system (Applied Biosystems), using the PowerUp SYBR Green Master Mix (Thermo Fisher Scientific). Gene-specific qPCR primers are listed in Table S8. Relative gene expression was calculated according to the ΔΔCt method (104), using *Actin 1* (*ACT1*; *YFL039C*) as the housekeeping gene for yeast and *Ubiquitin 10* (*UBQ10*; *At4g05320*) for Arabidopsis.

Histochemical GUS staining and plant imaging

GUS staining was carried out Arabidopsis seedlings on as described by (105). Plants were fixed in cold 90% (v/v) acetone 1 h, rinsed three times in 100 mM phosphate buffer and stained overnight at 37 °C in a GUS solution (0.2% Triton X-100, 2 mM potassium ferrocyanide, 2 mM potassium ferricyanide and 2 mM X-Gluc (5-bromo-4-chloro-3-indolyl b-D-glucuronide, sodium salt dissolved in DMSO) in 100 mM phosphate buffer, pH 7.2). Samples were washed in 70% ethanol prior to imaging. At the end of the staining (Fig. 3*C*) or the anoxic recovery (Fig. 3*B*), plants were imaged with a Leica THUNDER imager model organism using a bright field. FiJi was used for deconvolution of the plant images

ASBMB

treated with anoxia in their RGB channels, prior to measurement and quantification of integrated green pixel intensity within plant tissues.

In vitro *AtPCO4 inhibition assays*

Recombinant AtPCO4 was expressed and purified using Ni^{2+}-affinity and size exclusion chromatography, as described previously but including an additional protease cleavage step to remove the N-terminal His6 tag prior to size exclusion chromatography (5). AtPCO4 catalytic activity was measured by incubating recombinant enzyme (0.5 μM) with a synthetic 16mer peptide (GL Biochem, China) representing the Cys-initiating N-terminus of the AtERF-VII RAP2.12 (CGGAIISDFIPPPRSR, 500 μM) for 10 min at 25 °C prior to quenching with 1% formic acid. Assay mixtures also contained 20 μM FeSO4, 1 mM ascorbate and 5 mM TCEP in 50 mM Bis tris propane pH 8/40 mM NaCl. Oxidation was determined using RapidFire quadrupole time-of-flight mass spectrometry as described previously (106). Turnover was quantified by comparing the areas underneath the product and substrate ions. Spectra were manually assessed in Masshunter Qualitative Analysis B.07.00 (Agilent) to ensure the correct ion was chosen for quantification. Inhibition assays were determined by comparing activity as described above in the presence of 2A10 and 4D5 at a range of concentrations (1 μM - 5 mM). Compounds were preincubated with recombinant AtPCO4 for 10 min at 25 °C prior to substrate addition. Compounds were dissolved in DMSO therefore activity was normalized to DMSO-only controls. Data were plotted and IC50 values were generated using Prism (GraphPad). The HsADO inhibition assay in Fig. S7 was carried out with a synthetic 16mer peptide (GL Biochem, China) representing the Cys-initiating N-terminus of the HsRGS4 protein (CKGLAGLPASCLRSAK, 500 μM), using 0.25 μM recombinant ADO enzyme and following a method analogous to the AtPCO4 inhibition assays described above.

In silico *AtPCO4 molecular docking experiments*

AutoDockTools (version 1.5.7) provided as part of MGLTools (https://ccsb.scripps.edu/mgltools/downloads/), AutoDock Vina (version 1.2.1) (https://vina.scripps.edu/downloads/) and AutoDock4 (version 4.2.6) (https://autodock.scripps.edu/download-autodock4/) developed in the Molecular Graphics Lab at The Scripps Research Institute were installed for use in the following experiments.

To simulate 2A10 docking, the 3D structure of the 2A10 ligand was downloaded from PubChem database (https://pubchem.ncbi.nlm.nih.gov/) and AtPCO4 (PDB code: 6s7e, resolution 1.82 Å) was retrieved from RCSB Protein Data Bank (https://www.rcsb.org/). Both were prepared AutoDockTools. Docking experiments were preformed using default settings including energy range = 4, exhaustiveness = 8, and a grid box centered on the Fe atom (center coordinates: x = 33.429, y = 34.921, z = 18.621). An initial blind docking run used a grid box encompassing the entire enzyme (grid box coordinates: x = 66 Å, y = 70 Å, z = 46 Å). The lowest energy docking conformation featured 2A10 docked in the substrate binding pocket. A second docking run used a reduced search area focused on the substrate binding pocket (grid box coordinates: x = 22 Å, y = 16 Å, z = 22 Å). Results were visualized using PyMOL.

For $RAP_{2\text{-}8}$ docking experiments, AtPCO4 (PDB code: 6s7e, resolution 1.82 Å) was visualized in PyMOL and the 3× active site histidine residues (H98, H100, H164), and 3× H_2O molecules (molecule no.s 461, 498, 515) coordinated to the active site Fe were displayed. A peptide representing $RAP2.12_{2\text{-}8}$ (sequence: CGGAIIS, with C-terminus modified to an amide) was built and its N-terminal cysteine bound to the Fe, replacing H_2O 461. Steric clashes between the peptide and enzyme were minimized. The peptide and enzyme were prepared separately in AutoDockTools and assigned as a flexible region and rigid receptor respectively. Docking experiments were performed in the AutoDockTools graphical user interface using AutoDock4. The search parameters for the Genetic Algorithm were set to 10 runs and 250,000 maximum evaluations for initial trial experiments, and 100 runs and 2,500,000 maximum evaluations for the full experiments. A grid box encompassing the substrate binding pocket of the enzyme was constructed and Autogrid generated.map files required for docking. Docking outputs were visualized in PyMOL.

Data availability

All data discussed are contained within the manuscript.

Supporting information—This article contains supporting information.

Acknowledgments—We thank Roberta Sher for kind provision of the HsADO recombinant protein and Dr Anthony Tumber for assistance with RapidFire mass spectrometry.

Author contributions—M. L.-P, A. C., E. F., and B. G. conceptualization; R. L., M. L.-P., E. F., and B. G. methodology; R. L., M. L.-P., and F. B. investigation; R. L., M. L.-P., E. F., and B. G. writing-original draft; R. L., M. L.-P, E. F., and B. G. visualization; T. C., A. G., P. P., and A. C. writing–review & editing. A. G., P. P., and E. F. funding acquisition; A. C. resources. E. F. and B. G. supervision. B. G. project administration.

Funding and additional information—AC's research was funded by the "NextGenerationEU"/PRTR and the Spanish Ministry for Science and Innovation grants TED2021-129735B-I00 (MCIN/AEI/10.13039/501100011033). This research was partially funded by the "Fondazione Pisa, grant number 127/16" assigned to A. G. We thank the European Research Council (ERC) under the European Union's Horizon 2020 research and innovation program (PCO-MOD project, Grant Agreement 864888).

Conflict of interest—The authors declare that they have no conflicts of interest with the contents of this article.

Abbreviations—The abbreviations used are: AtPCO4, *Arabidopsis thaliana* Plant Cysteine Oxidase 4; BZ, bortezomib; CHX, cycloheximide; Cys-NDP, cysteine N-degron pathway; DLOR, Dual

Luciferase Oxygen Reporter; ERF-VII, Ethylene Response Factor VII; HTS, high-throughput screening.

References

1. Mohyeldin, A., Garzón-Muvdi, T., and Quiñones-Hinojosa, A. (2010) Oxygen in stem cell biology: a critical component of the stem cell niche. *Cell Stem Cell* **7**, 150–161
2. Weits, D. A., Kunkowska, A. B., Kamps, N. C. W., Portz, K. M. S., Packbier, N. K., Nemec Venza, Z., *et al.* (2019) An apical hypoxic niche sets the pace of shoot meristem activity. *Nature* **569**, 714–717
3. Shukla, V., Lombardi, L., Iacopino, S., Pencik, A., Novak, O., Perata, P., *et al.* (2019) Endogenous hypoxia in lateral root primordia controls root architecture by antagonizing auxin signaling in arabidopsis. *Mol. Plant* **12**, 538–551
4. Ehrismann, D., Flashman, E., Genn, D. N., Mathioudakis, N., Hewitson, K. S., Ratcliffe, P. J., *et al.* (2007) Studies on the activity of the hypoxia-inducible-factor hydroxylases using an oxygen consumption assay. *Biochem. J.* **401**, 227–234
5. White, M. D., Kamps, J. J. A. G., East, S., Taylor Kearney, L. J., and Flashman, E. (2018) The plant cysteine oxidases from Arabidopsis thaliana are kinetically tailored to act as oxygen sensors. *J. Biol. Chem.* **293**, 11786–11795
6. White, M. D., Klecker, M., Hopkinson, R. J., Weits, D. A., Mueller, C., Naumann, C., *et al.* (2017) Plant cysteine oxidases are dioxygenases that directly enable arginyl transferase-catalysed arginylation of N-end rule targets. *Nat. Commun.* **8**, 14690
7. Weits, D. A., Giuntoli, B., Kosmacz, M., Parlanti, S., Hubberten, H. M., Riegler, H., *et al.* (2014) Plant cysteine oxidases control the oxygen-dependent branch of the N-end-rule pathway. *Nat. Commun.* **5**, 3425
8. Bruick, R. K., and McKnight, S. L. (2001) A conserved family of prolyl-4-hydroxylases that modify HIF. *Science* **294**, 1337–1340
9. Epstein, A. C. R., Gleadle, J. M., McNeill, L. A., Hewitson, K. S., O'Rourke, J., Mole, D. R., *et al.* (2001) C. elegans EGL-9 and mammalian homologs define a family of dioxygenases that regulate HIF by prolyl hydroxylation. *Cell* **107**, 43–54
10. Dissmeyer, N. (2019) Conditional protein function via N-degron pathway–mediated Proteostasis in stress Physiology. *Annu. Rev. Plant Biol.* **70**, 83–117
11. Semenza, L. G. (1998) Hypoxia-inducible factor 1: master regulator of O2 homeostasis. *Curr. Opin. Genet. Dev.* **8**, 588–594
12. Gibbs, D. J., Lee, S. C., Md Isa, N., Gramuglia, S., Fukao, T., Bassel, G. W., *et al.* (2011) Homeostatic response to hypoxia is regulated by the N-end rule pathway in plants. *Nature* **479**, 415–418
13. Licausi, F., Kosmacz, M., Weits, D. A., Giuntoli, B., Giorgi, F. M., Voesenek, L. A. C. J., *et al.* (2011) Oxygen sensing in plants is mediated by an N-end rule pathway for protein destabilization. *Nature* **479**, 419–422
14. Hammarlund, E. U., Flashman, E., Mohlin, S., and Licausi, F. (2020) Oxygen-sensing mechanisms across eukaryotic kingdoms and their roles in complex multicellularity. *Science* **370**, eaba3512
15. Holdsworth, M. J., and Gibbs, D. J. (2020) Comparative biology of oxygen sensing in plants and animals. *Curr. Biol.* **30**, R362–R369
16. Schofield, C. J., and Ratcliffe, P. J. (2004) Oxygen sensing by HIF hydroxylases. *Nat. Rev. Mol. Cell Biol.* **5**, 343–354
17. Gunawardana, D. M., Heathcote, K. C., and Flashman, E. (2022) Emerging roles for thiol dioxygenases as oxygen sensors. *FEBS J.* **289**, 5426–5439
18. van Dongen, J. T., and Licausi, F. (2015) Oxygen sensing and signaling. *Annu. Rev. Plant Biol.* **66**, 345–367
19. Borisjuk, L., and Rolletschek, H. (2009) The oxygen status of the developing seed. *New Phytol.* **182**, 17–30
20. Joharapurkar, A. A., Pandya, V. B., Patel, V. J., Desai, R. C., and Jain, M. R. (2018) Prolyl hydroxylase inhibitors: a breakthrough in the therapy of anemia associated with Chronic Diseases. *J. Med. Chem.* **61**, 6964–6982
21. Fong, G. H., and Takeda, K. (2008) Role and regulation of prolyl hydroxylase domain proteins. *Cell Death Differ.* **15**, 635–641
22. Zhdanov, A. V., Okkelman, I. A., Collins, F. W. J., Melgar, S., and Papkovsky, D. B. (2015) A novel effect of DMOG on cell metabolism: direct inhibition of mitochondrial function precedes HIF target gene expression. *Biochim. Biophys. Acta* **1847**, 1254–1266
23. Su, K., Li, Z., Yu, Y., and Zhang, X. (2020) The prolyl hydroxylase inhibitor roxadustat: paradigm in drug discovery and prospects for clinical application beyond anemia. *Drug Discov. Today* **25**, 1262–1269
24. Yeh, T. L., Leissing, T. M., Abboud, M. I., Thinnes, C. C., Atasoylu, O., Holt-Martyn, J. P., *et al.* (2017) Molecular and cellular mechanisms of HIF prolyl hydroxylase inhibitors in clinical trials. *Chem. Sci.* **8**, 7651–7668
25. Figg, W. D., McDonough, M. A., Chowdhury, R., Nakashima, Y., Zhang, Z., Holt-Martyn, J. P., *et al.* (2021) Structural basis of prolyl hydroxylase domain inhibition by Molidustat. *ChemMedChem* **16**, 2082–2088
26. Chen, N., Hao, C., Peng, X., Lin, H., Yin, A., Hao, L., *et al.* (2019) Roxadustat for anemia in patients with kidney disease not receiving dialysis. *N. Engl. J. Med.* **381**, 1001–1010
27. Dhillon, S. (2019) Roxadustat: first Global Approval. *Drugs* **79**, 563–572
28. White, M. D., Dalle Carbonare, L., Lavilla Puerta, M., Iacopino, S., Edwards, M., Dunne, K., *et al.* (2020) Structures of Arabidopsis thaliana oxygen-sensing plant cysteine oxidases 4 and 5 enable targeted manipulation of their activity. *Proc. Natl. Acad. Sci. U. S. A.* **117**, 23140–23147
29. White, M. D., and Flashman, E. (2016) Catalytic strategies of the non-heme iron dependent oxygenases and their roles in plant biology. *Curr. Opin. Chem. Biol.* **31**, 126–135
30. Masson, N., Keeley, T. P., Giuntoli, B., White, M. D., Puerta, M. L., Perata, P., *et al.* (2019) Conserved N-terminal cysteine dioxygenases transduce responses to hypoxia in animals and plants. *Science* **69**, 65–69
31. Carbonare, L. D., White, M. D., Shukla, V., Francini, A., Perata, P., Flashman, E., *et al.* (2019) Zinc excess induces a hypoxia-like response by inhibiting cysteine oxidases in poplar roots. *Plant Physiol.* **180**, 1614–1628
32. Mendiondo, G. M., Gibbs, D. J., Szurman-Zubrzycka, M., Korn, A., Marquez, J., Szarejko, I., *et al.* (2016) Enhanced waterlogging tolerance in barley by manipulation of expression of the N-end rule pathway E3 ligase PROTEOLYSIS6. *Plant Biotechnol. J.* **14**, 40–50
33. Lin, C. C., Chao, Y. T., Chen, W. C., Ho, H. Y., Chou, M. Y., Li, Y. R., *et al.* (2019) Regulatory cascade involving transcriptional and N-end rule pathways in rice under submergence. *Proc. Natl. Acad. Sci. U. S. A.* **116**, 3300–3309
34. Weits, D. A., Zhou, L., Giuntoli, B., Carbonare, L. D., Iacopino, S., Piccinini, L., *et al.* (2022) Acquisition of hypoxia inducibility by oxygen sensing N-terminal cysteine oxidase in spermatophytes. *Plant Cell Environ.* **46**, 322–338
35. Chini, A., Monte, I., Fernandez-Barbero, G., Boter, M., Hicks, G., Raikhel, N., *et al.* (2021) A small molecule antagonizes jasmonic acid perception and auxin responses in vascular and nonvascular plants. *Plant Physiol.* **187**, 1399–1413
36. Chini, A. (2014) Application of yeast-two hybrid assay to chemical genomic screens: a high-throughput system to identify novel molecules modulating plant hormone receptor complexes. *Methods Mol. Biol.* **1056**, 35–43
37. Enserink, J. M. (2012) Chemical genetics: budding yeast as a platform for drug discovery and mapping of genetic pathways. *Molecules* **17**, 9258–9272
38. Puerta, M. L., Shukla, V., Dalle Carbonare, L., Weits, D. A., Perata, P., Licausi, F., *et al.* (2019) A ratiometric sensor based on plant N-terminal degrons able to Report oxygen dynamics in *Saccharomyces cerevisiae*. *J. Mol. Biol.* **431**, 2810–2820
39. Harris, A., Wagner, M., Du, D., Raschka, S., Nentwig, L. M., Gohlke, H., *et al.* (2021) Structure and efflux mechanism of the yeast pleiotropic drug resistance transporter Pdr5. *Nat. Commun.* **12**, 1–14
40. Balzi, E., Wang, M., Leterme, S., Van Dyck, L., and Goffeau, A. (1994) PDR5, a novel yeast multidrug resistance conferring transporter controlled by the transcription regulator PDR1. *J. Biol. Chem.* **269**, 2206–2214

ASBMB

41. Walsh, L., Hastwell, P. W., Keenan, P. O., Knight, A. W., Billinton, N., and Walmsley, R. M. (2005) Genetic modification and variations in solvent increase the sensitivity of the yeast RAD54-GFP genotoxicity assay. *Mutagenesis* **20**, 317–327
42. MacDonald, C., Winistorfer, S., Pope, R. M., Wright, M. E., and Piper, R. C. (2017) Enzyme reversal to explore the function of yeast E3 ubiquitin-ligases. *Traffic* **18**, 465–484
43. Emter, R., Heese-Peck, A., and Kralli, A. (2002) ERG6 and PDR5 regulate small lipophilic drug accumulation in yeast cells via distinct mechanisms. *FEBS Lett.* **521**, 57–61
44. Bard, M., Lees, N. D., Burrows, L. S., and Kleinhans, F. W. (1978) Differences in crystal violet uptake and cation-induced death among yeast sterol mutants. *J. Bacteriol.* **135**, 1146–1148
45. Welihinda, A. A., Beavis, A. D., and Trumbly, R. J. (1994) Mutations in LIS1 (ERG6) gene confer increased sodium and lithium uptake in *Saccharomyces cerevisiae*. *Biochim. Biophys. Acta* **1193**, 107–117
46. Simon, J. A., and Bedalov, A. (2004) Yeast as a model system for anticancer drug discovery. *Pharmacology* **4**, 475–560
47. Storici, F., and Resnick, M. A. (2006) The *Delitto Perfetto* approach to in vivo site-directed mutagenesis and chromosome rearrangements with synthetic oligonucleotides in yeast. *Methods Enzymol.* **409**, 329–345
48. Kamthan, A., Kamthan, M., and Datta, A. (2017) Expression of C-5 sterol desaturase from an edible mushroom in fisson yeast enhances its ethanol and thermotolerance. *PLoS One* **12**, 1–20
49. Watchaputi, K., Somboon, P., Phromma-in, N., Ratanakhanokchai, K., and Soontorngun, N. (2021) Actin cytoskeletal inhibitor 19,20-epoxycytochalasin Q sensitizes yeast cells lacking ERG6 through actin-targeting and secondarily through disruption of lipid homeostasis. *Sci. Rep.* **11**, 1–18
50. Zhang, N., Quan, Z., Rash, B., and Oliver, S. G. (2013) Synergistic effects of TOR and proteasome pathways on the yeast transcriptome and cell growth. *Open Biol.* **3**, 120137
51. Laborda, P., Alcalde-Rico, M., Chini, A., Martínez, J. L., and Hernando-Amado, S. (2021) Discovery of inhibitors of Pseudomonas aeruginosa virulence through the search for natural-like compounds with a dual role as inducers and substrates of efflux pumps. *Environ. Microbiol.* **23**, 7396–7411
52. Adoutte-Panvier, A., and Davies, J. E. (1984) Studies of ribosomes of yeast species: susceptibility to inhibitors of protein synthesis *in vivo* and *in vitro*. *Mol. Gen. Genet.* **194**, 310–317
53. Gladman, N. P., Marshall, R. S., Lee, K. H., and Vierstra, R. D. (2016) The proteasome stress regulon is controlled by a pair of NAC transcription factors in arabidopsis. *Plant Cell* **28**, 1279–1296
54. Banti, V., Mafessoni, F., Loreti, E., Alpi, A., and Perata, P. (2010) The heat-inducible transcription factor HsfA2 enhances anoxia tolerance in Arabidopsis. *Plant Physiol.* **152**, 1471–1483
55. Ventura, I., Brunello, L., Iacopino, S., Valeri, M. C., Novi, G., Dornbusch, T., *et al.* (2020) Arabidopsis phenotyping reveals the importance of alcohol dehydrogenase and pyruvate decarboxylase for aerobic plant growth. *Sci. Rep.* **10**, 1–14
56. Mustroph, A., Zanetti, M. E., Jang, C. J. H., Holtan, H. E., Repetti, P. P., Galbraith, D. W., *et al.* (2009) Profiling translatomes of discrete cell populations resolves altered cellular priorities during hypoxia in Arabidopsis. *Proc. Natl. Acad. Sci. U. S. A.* **106**, 18843–18848
57. Grillet, L., Lan, P., Li, W., Mokkapati, G., and Schmidt, W. (2018) IRON MAN is a ubiquitous family of peptides that control iron transport in plants. *Nat. Plants.* **4**, 953–963
58. Trott, O., and Olson, A. J. (2010) Software news and Update - AutoDock vina: improving the speed and accuracy of docking with a new scoring function, efficient optimization, and multithreading. *J. Comput. Chem.* **31**, 455–461
59. Eberhardt, J., Santos-Martins, D., Tillack, A. F., and Forli, S. (2021) AutoDock vina 1.2.0: new docking methods, expanded force field, and python bindings. *J. Chem. Inf. Model.* **61**, 3891–3898
60. Morris, G. M., Goodsell, D. S., Halliday, R. S., Huey, R., Hart, W. E., Belew, R. K., *et al.* (1998) Automated docking using a Lamarckian genetic algorithm and an empirical binding free energy function. *J. Comput. Chem.* **19**, 1639–1662
61. Milčić, N., Stepanić, V., Crnolatac, I., Findrik Blažević, Z., Brkljača, Z., and Majerić Elenkov, M. (2022) Inhibitory effect of DMSO on Haloalkohydrin Dehalogenase: experimental and computational insights into the influence of an organic Co-solvent on the structural and catalytic properties of a Biocatalyst. *Chemistry* **28**, e202201923
62. Misuri, L., Cappiello, M., Balestri, F., Moschini, R., Barracco, V., Mura, U., *et al.* (2017) The use of dimethylsulfoxide as a solvent in enzyme inhibition studies: the case of aldose reductase. *J. Enzyme Inhib. Med. Chem.* **32**, 1152–1158
63. Wang, Y., Shin, I., Li, J., and Liu, A. (2021) Crystal structure of human cysteamine dioxygenase provides a structural rationale for its function as an oxygen sensor. *J. Biol. Chem.* **279**, 101176
64. Fernandez, R. L., Elmendorf, L. D., Smith, R. W., Bingman, C. A., Fox, B. G., and Brunold, T. C. (2021) The crystal structure of cysteamine dioxygenase reveals the origin of the large substrate scope of this vital mammalian enzyme. *Biochemistry* **60**, 3728–3737
65. Chen, Z., Guo, Q., Wu, G., Wen, J., Liao, S., and Xu, C. (2021) Molecular basis for cysteine oxidation by plant cysteine oxidases from Arabidopsis thaliana. *J. Struct. Biol.* **213**, 107663
66. Pedersen, O., Perata, P., and Voesenek, L. A. C. J. (2017) Flooding and low oxygen responses in plants. *Funct. Plant Biol.* **44**, iii–vi
67. Taylor-Kearney, L. J., and Flashman, E. (2021) Targeting plant cysteine oxidase activity for improved submergence tolerance. *Plant J.* **109**, 779–788
68. Hartman, S., Sasidharan, R., and Voesenek, L. A. C. J. (2019) The role of ethylene in metabolic acclimations to low oxygen. *New Phytol.* **229**, 64–70
69. Bajorath, J. (2002) Chemoinformatics methods for systematic comparison of molecules from natural and synthetic sources and design of hybrid libraries. *J. Comput. Aided Mol. Des.* **16**, 431–439
70. Morales, P., Reggio, P. H., and Jagerovic, N. (2017) An overview on medicinal chemistry of synthetic and natural derivatives of cannabidiol. *Front. Pharmacol.* **8**, 1–18
71. Araniti, F., Mancuso, R., Lupini, A., Giofrè, S. V., Sunseri, F., Gabriele, B., *et al.* (2015) Phytotoxic potential and biological activity of three synthetic coumarin derivatives as new natural-like herbicides. *Molecules* **20**, 17883–17902
72. Atanasov, A. G., Zotchev, S. B., Dirsch, V. M., Orhan, I. E., Banach, M., Rollinger, J. M., *et al.* (2021) Natural products in drug discovery: advances and opportunities. *Nat. Rev. Drug Discov.* **20**, 200–216
73. Boldi, A. M. (2004) Libraries from natural product-like scaffolds. *Curr. Opin. Chem. Biol.* **8**, 281–286
74. Matilla, M. A., Daddaoua, A., Chini, A., Morel, B., and Krell, T. (2018) An auxin controls bacterial antibiotics production. *Nucleic Acids Res.* **46**, 11229–11238
75. Ceyhan, O., Birsoy, K., and Hoffman, C. S. (2012) Identification of biologically active pde11-selective inhibitors using a yeast-based high-throughput screen. *Chem. Biol.* **19**, 155–163
76. Griffioen, G., Duhamel, H., Van Damme, N., Pellens, K., Zabrocki, P., Pannecouque, C., *et al.* (2006) A yeast-based model of α-synucleinopathy identifies compounds with therapeutic potential. *Biochim. Biophys. Acta* **1762**, 312–318
77. Wong, L. H., Unciti-Broceta, A., Spitzer, M., White, R., Tyers, M., and Harrington, L. (2013) A yeast chemical genetic screen identifies inhibitors of human telomerase. *Chem. Biol.* **20**, 333–340
78. Gibbs, D. J., MdIsa, N., Movahedi, M., Lozano-Juste, J., Mendiondo, G. M., Berckhan, S., *et al.* (2014) Nitric oxide sensing in plants is mediated by proteolytic control of group VII ERF transcription factors. *Mol. Cell* **53**, 369–379
79. Manrique-Gil, I., Sánchez-Vicente, I., Torres-Quezada, I., and Lorenzo, O. (2021) Nitric oxide function during oxygen deprivation in physiological and stress processes. *J. Exp. Bot.* **72**, 904–916
80. Hartman, S., Liu, Z., van Veen, H., Vicente, J., Reinen, E., Martopawiro, S., *et al.* (2019) Ethylene-mediated nitric oxide depletion pre-adapts plants to hypoxia stress. *Nat. Commun.* **10**, 1–9
81. Holdsworth, M. J., Vicente, J., Sharma, G., Abbas, M., and Zubrycka, A. (2019) The plant N-degron pathways of ubiquitin-mediated proteolysis. *J. Integr. Plant Biol.* **62**, 70–89

82. Toussaint, M., and Conconi, A. (2006) High-throughput and sensitive assay to measure yeast cell growth: a bench protocol for testing genotoxic agents. *Nat. Protoc.* **1**, 1922–1928
83. Nourani, A., Wesolowski-Louvel, M., Delaveau, T., Jacq, C., and Delahodde, A. (1997) Multiple-drug-resistance phenomenon in the yeast Saccharomyces cerevisiae: involvement of two hexose transporters. *Mol. Cell. Biol.* **17**, 5453–5460
84. Scott, M., Gunderson, C. W., Mateescu, E. M., Zhang, Z., and Hwa, T. (2010) Interdependence of cell growth. *Science* **330**, 1099–1102
85. Krysan, D. J., and Didone, L. (2008) A high-throughput screening assay for small molecules that disrupt yeast cell integrity. *J. Biomol. Screen.* **13**, 657–664
86. Bauer, B. E., Wolfger, H., and Kuchler, K. (1999) Inventory and function of yeast ABC proteins: about sex, stress, pleiotropic drug and heavy metal resistance. *Biochim. Biophys. Acta* **1461**, 217–236
87. Stirke, A., Celiesiute-Germaniene, R., Zimkus, A., Zurauskiene, N., Simonis, P., Dervinis, A., *et al.* (2019) The link between yeast cell wall porosity and plasma membrane permeability after PEF treatment. *Sci. Rep.* **9**, 1–10
88. Egner, R., Rosenthal, F. E., Kralli, A., Sanglard, D., and Kuchler, K. (1998) Genetic separation of FK506 susceptibility and drug transport in the yeast PDr5 ATP-binding cassette multidrug resistance transporter. *Mol. Biol. Cell* **9**, 523–543
89. Gaber, R. F., Copple, D. M., Kennedy, B. K., Vidal, M., and Bard, M. (1989) The yeast gene ERG6 is required for normal membrane function but is not essential for biosynthesis of the cell-cycle-sparking sterol. *Mol. Cell. Biol.* **9**, 3447–3456
90. Kozlic, A., Winter, N., Telser, T., Reimann, J., Rose, K., Nehlin, L., *et al.* (2022) A yeast-based functional assay to study plant N-degron – N-recognin interactions. *Front. Plant Sci.* **12**, 1–12
91. Sriram, S., Lee, J. H., Mai, B. K., Jiang, Y., Kim, Y., Yoo, Y. D., *et al.* (2013) Development and characterization of monomeric N-end rule inhibitors through *in vitro* model substrates. *J. Med. Chem.* **56**, 2540–2546
92. Baker, R. T., and Varshavsky, A. (1991) Inhibition of the N-end rule pathway in living cells. *Proc. Natl. Acad. Sci. U. S. A.* **88**, 1090–1094
93. Lee, J. H., Jiang, Y., Kwon, Y. T., and Lee, M. J. (2015) Pharmacological modulation of the N-end rule pathway and its therapeutic Implications. *Trends Pharmacol. Sci.* **36**, 782–797
94. Rasheed, S., Rehman, K., Shahid, M., Suhail, S., and Akash, M. S. H. (2022) Therapeutic potentials of genistein: new insights and perspectives. *J. Food Biochem.* **46**, 1–16
95. Sohn, S. I., Pandian, S., Oh, Y. J., Kang, H. J., Cho, W. S., and Cho, Y. S. (2021) Metabolic engineering of isoflavones: an updated overview. *Front. Plant Sci.* **12**, 1–17
96. Ravishankar, D., Rajora, A. K., Greco, F., and Osborn, H. M. I. (2013) Flavonoids as prospective compounds for anti-cancer therapy. *Int. J. Biochem. Cell Biol.* **45**, 2821–2831
97. Nelson, K. J., Klomsiri, C., Codreanu, S. G., Soito, L., Liebler, D. C., Rogers, L. C., *et al.* (2010) Use of dimedone-based chemical Probes for sulfenic acid detection: methods to visualize and identify labeled proteins. *Methods Enzymol* **473**, 54–56
98. Gietz, R. D., and Schiestl, R. H. (2007) High-efficiency yeast transformation using the LiAc/SS carrier DNA/PEG method. *Nat. Protoc.* **2**, 31–34
99. Jung, P. P., Christian, N., Kay, D. P., Skupin, A., and Linster, C. L. (2015) Protocols and programs for high-throughput growth and aging phenotyping in yeast. *PLoS One* **10**, 1–20
100. Powell, E. O. (1956) Growth rate and generation time of Bacteria, with special reference to continuous culture. *J. Gen. Microbiol.* **15**, 492–511
101. Kosmacz, M., Parlanti, S., Schwarzländer, M., Kragler, F., Licausi, F., and Van Dongen, J. T. (2015) The stability and nuclear localization of the transcription factor RAP2.12 are dynamically regulated by oxygen concentration. *Plant Cell Environ.* **38**, 1094–1103
102. Schmitt, M. E., Brown, T. A., and Trumpower, B. L. (1990) A rapid and simple method for preparation of RNA from Saccharomyces cerevisiae. *Nucleic Acids Res.* **18**, 3091–3092
103. Bui, L. T., Giuntoli, B., Kosmacz, M., Parlanti, S., and Licausi, F. (2015) Constitutively expressed ERF-VII transcription factors redundantly activate the core anaerobic response in Arabidopsis thaliana. *Plant Sci.* **236**, 37–43
104. Kai, H., and Huiyun, F. (2001) Analysis of relative gene expression data using real- time quantitative PCR and the 2-DDCT method. *Methods* **25**, 402–408
105. Jefferson, R. A., Kavanagh, T. A., and Bevan, M. W. (1987) GUS fusions: beta-glucuronidase as a sensitive and versatile gene fusion marker in higher plants. *EMBO J.* **6**, 3901–3907
106. Taylor-Kearney, L. J., Madden, S., Wilson, J., Myers, W. K., Gunawardana, D. M., Pires, E., *et al.* (2022) Plant cysteine oxidase oxygen-sensing function is conserved in Early Land plants and Algae. *ACS Bio Med Chem Au* **2**, 521–528